

Handbook of Robotics

Chapter 27: Contact Modeling and Manipulation

Imin Kao

Department of Mechanical Engineering
State University of New York at Stony Brook
Stony Brook, New York 117940-2300, U.S.A.

Kevin Lynch

Department of Mechanical Engineering
Northwestern University
Evanston, IL 60208, USA

Joel Burdick

Department of Mechanical Engineering
California Institute of Technology
Pasadena, CA 91125, USA

September 15, 2007

Contents

27 Contact Modeling and Manipulation	1
27.1 Introduction	1
27.1.1 Overview	2
27.2 Kinematics of Rigid-Body Contact	2
27.2.1 Contact constraints	3
27.2.2 Collections of parts	4
27.2.3 Graphical planar methods	4
27.3 Forces and Friction	5
27.3.1 Graphical planar methods	7
27.3.2 Reciprocity of contact wrenches and twist	7
27.4 Rigid-Body Mechanics with Friction	8
27.4.1 Complementarity	8
27.4.2 Quasistatic assumption	8
27.4.3 Examples	8
27.5 Pushing Manipulation	10
27.6 Contact Interfaces and Modeling	12
27.6.1 Modeling of contact interface	12
27.6.2 Kinematic duality in contact modeling	13
27.6.3 Pressure distribution at contacts	14
27.7 Friction Limit Surface	15
27.7.1 Friction limit surface for point contact with friction	16
27.7.2 The friction limit surface at a soft contact interface	16
27.7.3 Example of constructing a friction limit surface	17
27.8 Contacts in Grasping and Fixture Designs	18
27.8.1 Contact stiffness of soft fingers	18
27.8.2 Application of soft contact theory to fixture design	19
27.9 Further Reading	19

Chapter 27

Contact Modeling and Manipulation

Robotic manipulators use contact forces to grasp and manipulate objects in their environments. Fixtures rely on contact to immobilize workpieces. Mobile robots and humanoids use wheels or feet to generate the contact forces that allow them to locomote. Modeling of the *contact interface*, therefore, is fundamental to analysis, design, planning, and control of many robotic tasks. This chapter presents an overview of the modeling of contact interfaces, with a particular focus on their use in manipulation tasks, including graspless or *nonprehensile* manipulation modes such as pushing. Analysis and design of grasps and fixtures also depends on contact modeling, and these are discussed in more detail in Chapter 28.

27.1 Introduction

A contact model characterizes both the forces that can be transmitted through the contact as well as the allowed relative motions of the contacting bodies. These characteristics are determined by the geometry of the contacting surfaces and the material properties of the parts, which dictate friction and possible contact deformation.

Choosing a Contact Model. The choice of a contact model largely depends upon the application or analysis that must be carried out. When appropriate analytical models are used, one can determine if a manipulation plan or fixture design meets desired functional requirements within the model's limits.

Rigid-body models. Many approaches to manipulation, grasp, and fixture analysis are based on rigid-body models. In the rigid-body model, no deformations are allowed at the points or surfaces of contact between two bodies. Instead, contact forces arise from two sources: the constraint of incompressibility and impenetrability between the rigid bodies, and surface frictional forces. Rigid-body models are straightforward to use, lead to

computationally efficient planning algorithms, and are compatible with solid-modeling software systems. Rigid-body models are often appropriate for answering qualitative questions such as “will this fixture be able to hold my workpiece?” and for problems involving stiff parts with low to moderate contact forces.

Rigid-body models are not capable of describing the full range of contact phenomena, however. For example, rigid-body models cannot predict the individual contact forces of a multiple-contact fixture (the static indeterminacy problem [8, 30]). Furthermore, workpieces held in fixtures experience non-negligible deformations in many high-force manufacturing operations [16, 17, 44, 45]. These deformations, which crucially impact machining accuracy, cannot be determined from rigid-body models. Also, a rigid-body model augmented with a Coulomb friction model can lead to mechanics problems that have no solution or multiple solutions [46, 47, 20, 23, 50, 62, 82, 55, 84]. To overcome the limitations inherent in the rigid-body model, one must introduce compliance into the contact model.

Compliant models. A *compliant* contact deforms under the influence of applied forces. The forces of interaction at the contact are derived from the *compliance* or *stiffness* model. While compliant contact models are typically more complicated, they have several advantages: they overcome the static indeterminacy inherent to rigid body models and they predict the deformations of grasped or fixtured parts during loading.

A detailed model of the deformations of real materials can be quite complex. Consequently, for analysis we often introduce *lumped parameter* or *reduced-order* compliance models having a limited number of variables. In this chapter we summarize a reduced-order *quasi-rigid-body* approach to modeling that can model a variety of compliant materials in a way that is consistent with both the solid mechanics literature and conventional robot analy-

sis and planning paradigms.

Finally, three-dimensional finite element models [77, 18, 86] or similar ideas [43, 79] can be used to analyze workpiece deformations and stresses in fixtures. While accurate, these numerical approaches have some drawbacks. For example, the grasp stiffness matrix can only be found through difficult numerical procedures. Stiffness matrices are often needed to compute quality measures that are the basis for optimal grasping plans or fixturing designs [59, 63]. Thus, these numerical approaches are better suited for verifying final fixture designs.

Grasp/Manipulation Analysis. Once a contact model has been chosen, we can use it to analyze tasks involving multiple contacts. If a part is subject to multiple contacts, the kinematic constraints and force freedoms due to the individual contacts must be combined. This combined analysis facilitates manipulation planning—choosing the contact locations, and possibly the motions or forces applied by those contacts, to achieve the desired behavior of the part. A prime example is the grasping or fixturing problem: choosing contact locations, and possibly contact forces, to prevent motion of a part in the face of external disturbances. This well-studied topic is discussed in greater detail in Chapter 28. Other examples include problems of partial constraint, such as pushing a part or inserting a peg into a hole.

27.1.1 Overview

Sections 27.2–27.5 focus on rigid-body models of contact. Section 27.2 describes the kinematic constraints caused by contact, and Section 27.3 describes the contact forces that may arise with Coulomb friction. Section 27.4 provides examples of analysis of multi-contact manipulation tasks with rigid bodies and Coulomb friction. Section 27.5 shows how the limit surface can be used to analyze pushing problems. Section 27.6 introduces modeling of contact interfaces, kinematic duality and pressure distribution. Section 27.7 describes the concept of friction limit surface and illustrates with an example for the constructing such surface of a soft contact. Finally, Section 27.8 discusses how these more accurate models can be used in fixture analysis and design.

27.2 Kinematics of Rigid-Body Contact

Contact kinematics is the study of how two or more parts can move relative to each other while respecting

the rigid-body impenetrability constraint. It also classifies motion in contact as either rolling or slipping.

Consider two rigid bodies whose position and orientation (configuration) is given by the local coordinate column vectors \mathbf{q}_1 and \mathbf{q}_2 , respectively. Writing the composite configuration as $\mathbf{q} = [\mathbf{q}_1^T, \mathbf{q}_2^T]^T$, we define a “distance” function $d(\mathbf{q})$ between the parts that is positive when they are separated, zero when they are touching, and negative when they are in penetration. When $d(\mathbf{q}) > 0$, there are no constraints on the motions of the parts. When the parts are in contact ($d(\mathbf{q}) = 0$), we look at the time derivatives \dot{d} , \ddot{d} , etc., to determine if the parts stay in contact or break apart as they follow a trajectory $\mathbf{q}(t)$. This can be determined by the following table of possibilities:

d	\dot{d}	\ddot{d}	...	
> 0				no contact
< 0				infeasible (penetration)
$= 0$	> 0			breaking contact
$= 0$	< 0			infeasible (penetration)
$= 0$	$= 0$	> 0		breaking contact
$= 0$	$= 0$	< 0		infeasible (penetration)
				etc.

The contact is maintained only if all time derivatives are zero.

The first two time derivatives are written

$$\dot{d} = \left(\frac{\partial d}{\partial \mathbf{q}} \right)^T \dot{\mathbf{q}} \quad (27.1)$$

$$\ddot{d} = \dot{\mathbf{q}}^T \frac{\partial^2 d}{\partial \mathbf{q}^2} \dot{\mathbf{q}} + \left(\frac{\partial d}{\partial \mathbf{q}} \right)^T \ddot{\mathbf{q}}. \quad (27.2)$$

The terms $\partial d / \partial \mathbf{q}$ and $\partial^2 d / \partial \mathbf{q}^2$ carry information about the local contact geometry. The former corresponds to the contact normal, while the latter corresponds to the relative curvature of the parts at the contact.

If contact is maintained, we can classify the contact as slipping or rolling. Analogous to the table above, the contact is rolling if and only if there is zero relative tangential velocity, acceleration, etc., between the contact points on the parts. If the relative tangential velocity is nonzero, the parts are slipping; if the relative velocity is zero but relative tangential acceleration or (higher-order derivatives) is not, slipping is incipient.

In this section we focus on a *first-order* analysis of contact kinematics. A first-order analysis concludes that contact is maintained if $d(\mathbf{q}) = 0$ and $\dot{d} = 0$. This local “linearization” of contact kinematics focuses on the velocity $\dot{\mathbf{q}}$ and the contact normal in $\partial d / \partial \mathbf{q}$; higher-order

spatial derivatives of the contact geometry (curvature, etc.) are not considered. While this is a good starting point, it may occasionally lead to erroneous conclusions. For example, Rimon and Burdick [71, 72, 73] showed that a first-order analysis may incorrectly predict mobility of a part in a fixture when a second-order analysis shows that it is in fact completely constrained.

Analysis of the kinematics of rolling contact of parameterized surfaces can be found in [57]; see also [12, 11, 13, 58].

27.2.1 Contact constraints

As described in Chapter 1, a rigid body in space has six degrees of freedom, specified by the location of the origin of a coordinate frame P affixed to the part and the orientation of this coordinate frame relative to an inertial frame O fixed in the world. Let ${}^O\mathbf{p}_P \in \mathbb{R}^3$ be the position of the part center of mass and ${}^O\mathbf{R}_P \in SO(3)$ be the rotation matrix describing the orientation of the part relative to O . The spatial velocity of the part can be written as $\mathbf{t} \in \mathbb{R}^6$, sometimes called a *twist*,

$$\mathbf{t} = [\boldsymbol{\omega}^T, \mathbf{v}^T]^T,$$

where $\boldsymbol{\omega} = [\omega_x, \omega_y, \omega_z]^T$ and $\mathbf{v} = [v_x, v_y, v_z]^T$ give the angular velocity and linear velocity of P in the world frame O , respectively, such that $\boldsymbol{\omega}$ satisfies

$${}^O\dot{\mathbf{R}}_P = \boldsymbol{\omega} \times {}^O\mathbf{R}_P$$

and \mathbf{v} satisfies

$$\mathbf{v} = {}^O\dot{\mathbf{p}}_P - \boldsymbol{\omega} \times {}^O\mathbf{p}_P.$$

It is worth taking a moment to really understand the spatial velocity of a body. It consists of the body's angular velocity expressed in the world frame O , along with the linear velocity of a point as if it were rigidly attached to the body but currently at the origin of the world frame. This point need not be physically on the body. In other words, \mathbf{v} is not simply ${}^O\dot{\mathbf{p}}_P$. This notation will simplify the following expressions, where all velocities and forces will be expressed in the common world frame O . (Be aware that twists are sometimes defined in a body frame instead.)

A point contact acting on the part provides a unilateral constraint which prevents the part from locally moving against the contact normal. Let \mathbf{x} be the location of the contact in O . The linear velocity of the point on the part in contact is

$$\mathbf{v}_C = \mathbf{v} + \boldsymbol{\omega} \times \mathbf{x}.$$

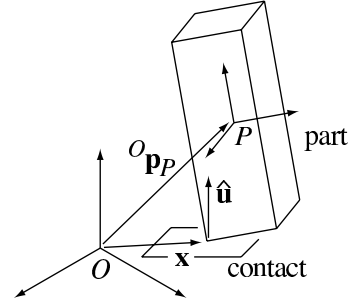


Figure 27.1: Notation for a part in contact with a manipulator or the environment.

(We drop the pre-superscripts O for simplicity; for example, ${}^O\mathbf{x}$ is written simply as \mathbf{x} .) Let $\hat{\mathbf{u}}$ be the unit vector normal pointing into the part (Figure 27.1). The first-order condition that the part not move into the unilateral constraint can be written

$$\mathbf{v}_C^T \hat{\mathbf{u}} = (\mathbf{v} + \boldsymbol{\omega} \times \mathbf{x})^T \hat{\mathbf{u}} \geq 0. \quad (27.3)$$

In other words, the velocity of the part at C cannot have a component in the opposite direction of the contact normal. To write this another way, define a generalized force or *wrench* \mathbf{w} consisting of the torque \mathbf{m} and force \mathbf{f} acting on the part for a unit force along the contact normal:

$$\mathbf{w} = [\mathbf{m}^T, \mathbf{f}^T]^T = [(\mathbf{x} \times \hat{\mathbf{u}})^T, \hat{\mathbf{u}}^T]^T.$$

Then (27.3) can be rewritten as

$$\mathbf{t}^T \mathbf{w} \geq 0. \quad (27.4)$$

If the external constraint point is moving with linear velocity \mathbf{v}_{ext} , (27.4) changes to

$$\mathbf{t}^T \mathbf{w} \geq \mathbf{v}_{\text{ext}}^T \hat{\mathbf{u}}, \quad (27.5)$$

which reduces to (27.4) if the constraint is stationary.

Each inequality of the form (27.5) constrains the velocity of the part to a half-space of its six-dimensional velocity space bounded by the hyperplane $\mathbf{t}^T \mathbf{w} = \mathbf{v}_{\text{ext}}^T \hat{\mathbf{u}}$. Unioning the set of all constraints, we get a convex polyhedral set of feasible part velocities. A constraint is redundant if its half-space constraint does not change the feasible velocity polyhedron. For a given twist \mathbf{t} , a constraint is active if

$$\mathbf{t}^T \mathbf{w} = \mathbf{v}_{\text{ext}}^T \hat{\mathbf{u}}; \quad (27.6)$$

otherwise the part is breaking contact at that point. In general, the feasible velocity polyhedron for a part

can consist of a six-dimensional interior (where no contact constraint is active), five-dimensional hyperfaces, four-dimensional hyperfaces, and so on, down to one-dimensional edges and zero-dimensional points. A part velocity on an n -dimensional facet of the velocity polyhedron indicates that $6 - n$ independent (non-redundant) constraints are active.

If all of the constraints are stationary ($\mathbf{v}_{\text{ext}} = \mathbf{0}$), then each constraining half-plane defined by (27.5) passes through the origin of the velocity space, and the feasible velocity set becomes a cone rooted at the origin. Let \mathbf{w}_i be the constraint wrench of stationary contact i . Then the feasible velocity cone is

$$V = \{\mathbf{t} \mid \mathbf{t}^T \mathbf{w}_i \geq 0 \ \forall i\}.$$

If the \mathbf{w}_i span the six-dimensional generalized force space, or, equivalently, the convex hull of the \mathbf{w}_i contains the origin in the interior, then the stationary contacts completely constrain the motion of the part, and we have form closure, as discussed in Chapter 28.

In the discussion above, each constraint (27.5) divides the part velocity space into three categories: a hyperplane of velocities that maintain contact, a half-space of velocities that separate the parts, and a half-space of velocities that cause the parts to penetrate. Velocities where the contact is maintained can be further broken down into two categories: velocities where the part slips over the contact constraint, and velocities where the part sticks or rolls on the constraint. In the latter case, the part velocity satisfies the three equations

$$\mathbf{v} + \boldsymbol{\omega} \times \mathbf{x} = \mathbf{v}_{\text{ext}}. \quad (27.7)$$

Now we can give each point contact i a label m_i corresponding to the type of contact, called the contact label: \mathbf{b} if the contact is breaking, \mathbf{f} if the contact is fixed (including rolling), and \mathbf{s} if the contact is slipping, i.e., (27.6) is satisfied but (27.7) is not. The *contact mode* for the entire system can be written as the concatenation of the contact labels at the k contacts, $m_1 m_2 \dots m_k$.

27.2.2 Collections of parts

The discussion above can be generalized to find the feasible velocities of multiple parts in contact. If parts i and j make contact at a point \mathbf{x} , where $\hat{\mathbf{u}}_i$ points into part i and $\mathbf{w}_i = [(\mathbf{x} \times \hat{\mathbf{u}}_i)^T, \hat{\mathbf{u}}_i^T]^T$, then their spatial velocities \mathbf{t}_i and \mathbf{t}_j must satisfy the constraint

$$(\mathbf{t}_i - \mathbf{t}_j)^T \mathbf{w}_i \geq 0 \quad (27.8)$$

to avoid penetration. This is a homogeneous half-space constraint in the composite $(\mathbf{t}_i, \mathbf{t}_j)$ velocity space. In an assembly of multiple parts, each pairwise contact contributes another constraint in the composite part velocity space, and the result is a polyhedral convex cone of kinematically feasible velocities rooted at the origin of the composite velocity space. The contact mode for the entire assembly is the concatenation of the contact labels at each contact in the assembly.

If there are moving contacts whose motion is prescribed, e.g., robot fingers, the constraints on the motion of the remaining parts will no longer be homogeneous. As a result, the convex polyhedral feasible velocity space is no longer a cone rooted at the origin.

27.2.3 Graphical planar methods

When a part is confined to move in the xy plane, the twist \mathbf{t} reduces to $\mathbf{t} = [\omega_x, \omega_y, \omega_z, v_x, v_y, v_z]^T = [0, 0, \omega_z, v_x, v_y, 0]^T$. The point $(-v_y/\omega_z, v_x/\omega_z)$ is called the center of rotation (COR) in the projective plane, and we can represent any planar twist by its COR and rotational velocity ω_z .¹ This is sometimes useful for graphical purposes: for a single part constrained by stationary fixtures, at least, we can easily draw the feasible twist cone as CORs [55, 67].

As an example, Figure 27.2(a) shows a planar part standing on a table and being contacted by a robot finger. This finger is currently stationary, but we will later set it in motion. The finger defines one constraint on the part's motion and the table defines two more. (Note that contact points in the interior of the edge between the part and the table provide redundant kinematic constraints.) The constraint wrenches can be written

$$\begin{aligned} \mathbf{w}_1 &= [0, 0, -1, 0, 1, 0]^T \\ \mathbf{w}_2 &= [0, 0, 1, 0, 1, 0]^T \\ \mathbf{w}_3 &= [0, 0, 1, -1, 0, 0]^T. \end{aligned}$$

For a stationary finger, the kinematic constraints yield the feasible twist cone shown in Figure 27.2(b). This region can also be easily visualized in the plane by using the following method: at each contact, draw the contact normal line. Label all points on the normal \pm , points to the left of the inward normal $+$, and points to the right $-$. For each contact constraint, all the points labeled $+$ can serve as CORs with positive angular velocity, and all the points labeled $-$ can serve as CORs with

¹Note that the case $\omega_z = 0$ must be treated with care, as it corresponds to a COR at infinity.

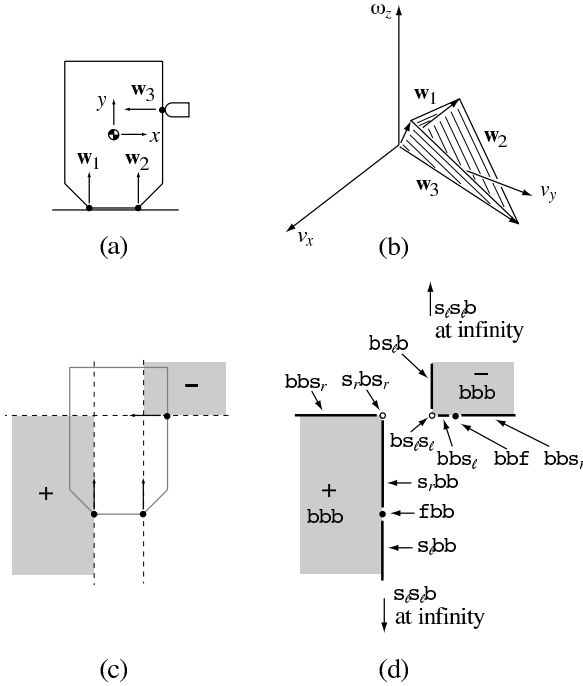


Figure 27.2: (a) A part resting on a table and the three contact constraints. (b) The twist cone satisfying the contact constraints. The contact normals are shown with their associated constraint planes. (c) The equivalent representation as CORs, shown in grey. Note that the lines that extend off to the left and to the bottom “wrap around” at infinity and come back in from the right and the top, respectively, so this COR region should be interpreted as a single connected convex region, equivalent to the twist cone representation in (b). (d) The contact modes assigned to each feasible motion. The zero velocity contact mode is *fff*.

negative angular velocity, without violating the contact constraint. After doing this for all the contact normals, keep only the CORs that are consistently labeled. These CORs are a planar representation of the feasible twist cone (Figure 27.2(c)).

We can refine this method by assigning contact modes to each feasible COR. For each contact normal, label the COR at the contact point *f* for fixed, other CORs on the normal line *s* for slipping, and all other CORs *b* for breaking contact. The concatenation of these labels gives the part’s contact mode for a particular part motion. In the planar case, the label *s* on the contact normal line can be further refined into *s_r* or *s_ℓ* indicating whether the

part is slipping right or left relative to the constraint. An *s* COR labeled + “above” the contact (in the direction of the contact normal) or – below the contact should be relabeled *s_r* and an *s* COR labeled – above the contact or + below should be relabeled *s_ℓ* (Figure 27.2(d)).

This method can be used readily to determine if the part is in form closure. If there is no COR labeled consistently, then the feasible velocity cone consists of only the zero velocity point, and the part is immobilized by the stationary contacts. This method also makes it clear that at least four contacts are necessary to immobilize the part by the first-order analysis (see also Chapter 28). This is a weakness of the first-order analysis—curvature effects can be used to immobilize a part with three or even two contacts [72]. This weakness can also be seen in Figure 27.2(d). A pure rotation about the COR labeled {+, *s_rbs_r*} is actually not feasible, but it would be if the part had a small radius of curvature at the contact with the finger. The first-order analysis ignores this curvature.

27.3 Forces and Friction

A commonly-used model of friction in robotic manipulation is Coulomb’s law [15]. This experimental law states that the friction force magnitude *f_t* in the tangent plane at the contact interface is related to the normal force magnitude *f_n* by *f_t ≤ μf_n*, where *μ* is called the friction coefficient. If the contact is sliding, then *f_t = μf_n*, and the friction force opposes the direction of motion. The friction force is independent of the speed of sliding.

Often two friction coefficients are defined, a static friction coefficient *μ_s* and a kinetic (or sliding) friction coefficient *μ_k*, where *μ_s ≥ μ_k*. This implies that a larger friction force is available to resist initial motion, but once motion has begun, the resisting force decreases. Many other friction models have been developed with different functional dependences on factors such as the speed of sliding and the duration of static contact before sliding. All of these are aggregate models of complex microscopic behavior. For simplicity, we will assume the simplest Coulomb friction model with a single friction coefficient *μ*. This model is reasonable for hard, dry materials. The friction coefficient depends on the two materials in contact, and typically ranges from 0.1 to 1.

Figure 27.3(a) shows that this friction law can be interpreted in terms of a *friction cone*. The set of all forces that can be applied to the disk by the supporting line is constrained to be inside this cone. Correspondingly, any

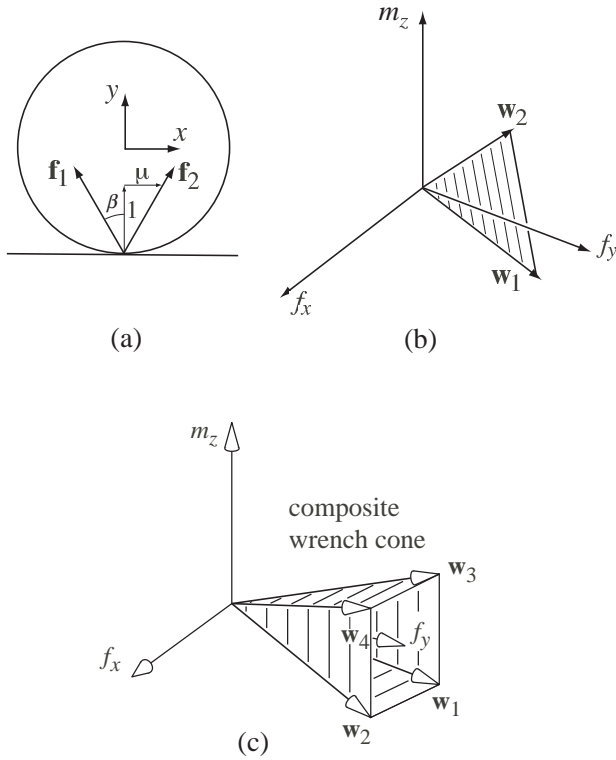


Figure 27.3: (a) A planar friction cone. (b) The corresponding wrench cone. (c) An example composite wrench cone resulting from two frictional contacts.

force the disk applies to the support is inside the negative of the cone. The half-angle of the cone is $\beta = \tan^{-1} \mu$, as shown in Figure 27.4. If the disk slips to the left on the support, the force the support applies to it acts on the right edge of the friction cone, with a magnitude determined by the normal force.

If we choose a coordinate frame, the force \mathbf{f} applied to the disk by the support can be expressed as a wrench $\mathbf{w} = [(\mathbf{x} \times \mathbf{f})^T, \mathbf{f}^T]^T$, where \mathbf{x} is the contact location. Thus the friction cone turns into a wrench cone, as shown in Figure 27.3(b). The two edges of the planar friction cone give two half-lines in the wrench space, and the wrenches that can be transmitted to the part through the contact are all nonnegative linear combinations of basis vectors along these edges. If \mathbf{w}_1 and \mathbf{w}_2 are basis vectors for these wrench cone edges, we write the wrench cone as

$$\mathcal{WC} = \{k_1 \mathbf{w}_1 + k_2 \mathbf{w}_2 \mid k_1, k_2 \geq 0\}.$$

If there are multiple contacts acting on a part, then

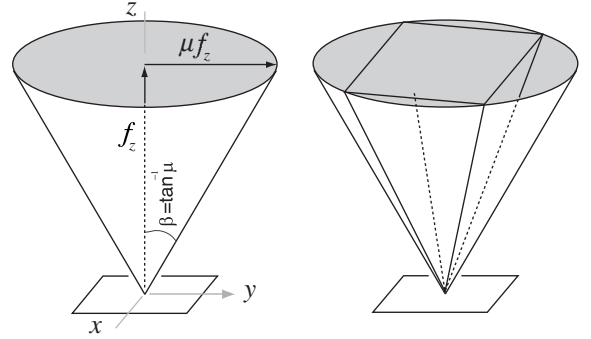


Figure 27.4: (Left) A spatial friction cone. The half-angle of the cone is $\beta = \tan^{-1} \mu$. (Right) An inscribed pyramidal approximation to the friction cone. A more accurate inscribed pyramidal approximation can be used by increasing the number of faces of the pyramid. Depending on the application, a circumscribed pyramid could be used instead of an inscribed pyramid.

the total set of wrenches that can be transmitted to the part through the contacts is the nonnegative linear combination of all the individual wrench cones \mathcal{WC}_i ,

$$\mathcal{WC} = \text{pos}(\{\mathcal{WC}_i\}) = \left\{ \sum_i k_i \mathbf{w}_i \mid \mathbf{w}_i \in \mathcal{WC}_i, k_i \geq 0 \right\}.$$

This composite wrench cone is a convex polyhedral cone rooted at the origin. An example composite wrench cone arising from two planar frictional contacts is shown in Figure 27.3(c). If the composite wrench cone is the entire wrench space, then the contacts can provide a force closure grasp (Chapter 28).

In the spatial case, the friction cone is a circular cone, defined by

$$\sqrt{f_x^2 + f_y^2} \leq \mu f_z, \quad f_z \geq 0 \quad (27.9)$$

when the contact normal is in the $+z$ direction (Figure 27.4). The resulting wrench cone, and composite wrench cone $\text{pos}(\{\mathcal{WC}_i\})$ for multiple contacts, is a convex cone rooted at the origin, but it is not polyhedral. For computational purposes, it is common to approximate circular friction cones as pyramidal cones, as shown in Figure 27.4. Then individual and composite wrench cones become polyhedral convex cones in the six-dimensional wrench space.

If a contact or set of contacts acting on a part is ideally force-controlled, the wrench \mathbf{w}_{ext} specified by the controller must lie within the composite wrench cone

corresponding to those contacts. Because these force-controlled contacts choose a subset of wrenches (possibly a single wrench) from this wrench cone, the total composite wrench cone that can act on the part (including other non-force-controlled contacts) may no longer be a homogeneous cone rooted at the origin. This is roughly analogous to the case of position-controlled contacts in Section 27.2.1, which results in a feasible twist set for the part that is not a cone rooted at the origin. Ideal robot manipulators may be controlled by position control, force control, hybrid position-force control, or some other scheme. The control method must be compatible with the parts' contacts with each other and the environment to prevent excessive forces [52].

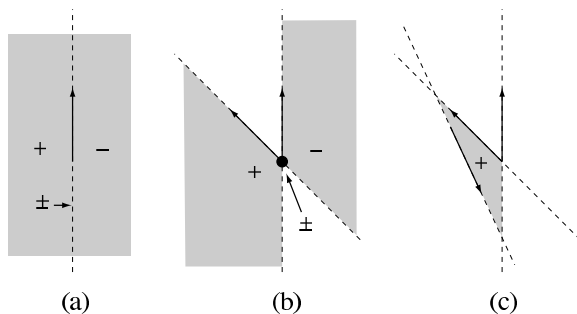


Figure 27.5: (a) Representing a line of force by moment labels. (b) Representing the nonnegative linear combinations of two lines of force by moment labels. (c) Non-negative linear combinations of three lines of force.

27.3.1 Graphical planar methods

Just as homogeneous twist cones for planar problems can be represented as convex signed (+ or -) COR regions in the plane, homogeneous wrench cones for planar problems can be represented as convex signed regions in the plane. This is called *moment labeling* [54, 55]. Given a collection of lines of force in the plane (e.g., the edges of friction cones from a set of point contacts), the set of all nonnegative linear combinations of these can be represented by labeling all the points in the plane with either a '+' if all resultants make nonnegative moment about that point, a '-' if all make nonpositive moment about that point, a '±' if all make zero moment about that point, and a blank label if there exist resultants making positive moment and resultants making negative moment about that point.

The idea is best illustrated by an example. In Figure 27.5(a), a single line of force is represented by labeling the points to the left of the line with a + and points to the right of the line with a -. Points on the line are labeled ±. In Figure 27.5(b), another line of force is added. Only the points in the plane that are consistently labeled for both lines of force retain their labels; inconsistently labeled points lose their labels. Finally, a third line of force is added in Figure 27.5(c). The result is a single region labeled +. A nonnegative combination of the three lines of force can create any line of force in the plane that passes around this region in a counterclockwise sense. This representation is equivalent to a homogeneous convex wrench cone representation.

27.3.2 Reciprocity of contact wrenches and twist

Our discussion of kinematic constraints and friction should make apparent that, for any point contact and contact label, the number of equality constraints on the part's motion caused by that contact is equal to the number of wrench freedoms it provides. For example, a breaking contact **b** provides zero equality constraints on the part motion and also allows no contact force. A fixed contact **f** provides 3 motion constraints (the motion of a point on the part is specified) and 3 freedoms on the contact force: any wrench in the interior of the contact wrench cone is consistent with the contact mode. Finally, a slipping contact **s** provides 1 equality motion constraint (one equation on the part's motion must be satisfied to maintain the contact), and for a given motion satisfying the constraint, the contact wrench has only 1 freedom, the magnitude of the contact wrench on the edge of the friction cone and opposite the slipping direction. In the planar case, the motion constraints and wrench freedoms for **b**, **s**, and **f** contacts are 0, 1, and 2, respectively.

Consider, for example, a stationary constraint contacting a part at $\mathbf{x} = \mathbf{0}$, with a contact normal $\hat{\mathbf{u}} = [0, 0, 1]^T$. Assume the normal force into the part satisfies $f_z > 0$ so the contact is maintained. Three canonical contact types are discussed further in Section 27.6.2.

27.4 Rigid-Body Mechanics with Friction

The manipulation planning problem is to choose the motions or forces applied by manipulator contacts so that the part (or parts) move as desired. This requires solving the subproblem of determining the motion of parts given a particular manipulator action.

Let $\mathbf{q} \in \mathbb{R}^n$ be local coordinates describing the combined configuration of the system consisting of one or more parts and robot manipulators, and let $\mathbf{w}_i \in \mathbb{R}^6$ represent a wrench at an active contact i , measured in the common coordinate frame O . Let $\mathbf{w}_{\text{all}} \in \mathbb{R}^{6k}$ be the vector obtained by stacking the \mathbf{w}_i , $\mathbf{w}_{\text{all}} = [\mathbf{w}_1^T \ \mathbf{w}_2^T \ \dots \ \mathbf{w}_k^T]^T$ (where there are k contacts), and let $\mathbf{A}(\mathbf{q}) \in \mathbb{R}^{n \times 6k}$ be a matrix indicating how (or if) each contact wrench acts on each part. (Note that a contact wrench \mathbf{w}_i acting on one part means that there is a contact wrench $-\mathbf{w}_i$ acting on the other part in contact.) The problem is to find the contact forces \mathbf{w}_{all} and the system acceleration $\ddot{\mathbf{q}}$, given the state of the system $(\mathbf{q}, \dot{\mathbf{q}})$, the system mass matrix $\mathbf{M}(\mathbf{q})$ and resulting Coriolis matrix $\mathbf{C}(\mathbf{q}, \dot{\mathbf{q}})$, the gravitational forces $\mathbf{g}(\mathbf{q})$, the control forces $\boldsymbol{\tau}$, and the matrix $\mathbf{T}(\mathbf{q})$ indicating how the control forces $\boldsymbol{\tau}$ act on the system. (Alternatively, if we view the manipulators as position-controlled, the manipulator components of $\ddot{\mathbf{q}}$ can be directly specified and the corresponding components of the control forces $\boldsymbol{\tau}$ solved for.) One way to solve this problem is to (a) enumerate the set of all possible contact modes for the current active contacts, and (b) for each contact mode, determine if there are wrenches \mathbf{w}_{all} and accelerations $\ddot{\mathbf{q}}$ that satisfy the dynamics

$$\mathbf{A}(\mathbf{q})\mathbf{w}_{\text{all}} + \mathbf{T}(\mathbf{q})\boldsymbol{\tau} - \mathbf{g}(\mathbf{q}) = \mathbf{M}(\mathbf{q})\ddot{\mathbf{q}} + \mathbf{C}(\mathbf{q}, \dot{\mathbf{q}})\dot{\mathbf{q}} \quad (27.10)$$

and are consistent with the contact mode's kinematic constraints (constraints on $\dot{\mathbf{q}}$) and friction cone force constraints (constraints on \mathbf{w}_{all}). This formulation is quite general and applies to multiple parts in contact. The equation (27.10) may be simplified by appropriate representations of the configurations and velocities of rigid-body parts (for example, using angular velocities of the rigid bodies instead of derivatives of local angular coordinates).

This formulation leads to some surprising conclusions: there may be multiple solutions to a particular problem (ambiguity) or there may be no solutions (inconsistency) [46, 47, 20, 23, 50, 62, 82, 55]. This strange behavior arises from the status of Coulomb's law as an approximate law, and it disappears for zero friction, or

friction that is “small enough.” Despite this weakness of the Coulomb friction law, it is a useful approximation. Nonetheless, if we would like to prove (under the Coulomb model) that a particular desired part motion occurs, we generally must also show that no other motion can occur. Otherwise we have only shown that the desired motion is one of the possible outcomes.

27.4.1 Complementarity

The conditions that each contact provides an equal number of motion constraints and wrench freedoms (Section 27.3.2) can be written as *complementarity* conditions. Thus the problem of solving (27.10), subject to contact constraints, can be formulated as a complementarity problem (CP) [3, 5, 62, 76, 78, 82]. For planar problems, or spatial problems with approximate pyramidal friction cones, the problem is a linear complementarity problem [14]. For circular spatial friction cones, the problem is a nonlinear complementarity problem, due to the quadratic constraints describing the cones. In either case, standard algorithms can be used to solve for possible contact modes and part motions.

Alternatively, assuming linearized friction cones, we can formulate a linear constraint satisfaction program (LCSP) for each contact mode (e.g., a linear program with no objective function). The contact mode places linear constraints on the part accelerations, and the solver solves for the part accelerations and the nonnegative coefficients multiplying each of the edges of the friction cones, subject to the dynamics (27.10). Each LCSP with a feasible solution represents a feasible contact mode.

27.4.2 Quasistatic assumption

A common assumption in robot manipulation planning is the *quasistatic* assumption. This assumption says that parts move slowly enough that inertial effects are negligible. This means that the right and left hand sides of (27.10) are zero. With this assumption, we often solve for part *velocities* rather than accelerations. These velocities must be consistent with the kinematic constraints and force constraints, and forces acting on the parts must always sum to zero.

27.4.3 Examples

While rigid-body mechanics problems with friction are usually solved using computational tools for CP's and

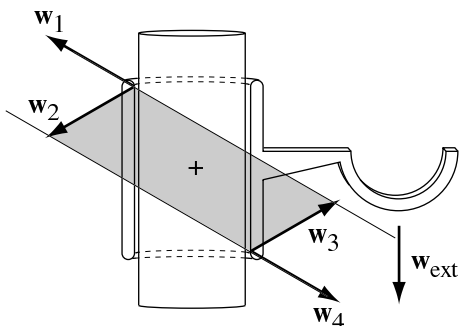


Figure 27.6: The moment-labeling representation of the composite wrench cone of contact forces the pipe can apply to the pipe clamp. In this figure, the wrench \mathbf{w}_{ext} applied to the pipe clamp can be resisted by forces within the composite wrench cone.

LCSP's, equivalent graphical methods can be used for some planar problems to assist the intuition. As a simple example, consider the pipe clamp in Figure 27.6 [55]. Under the external wrench \mathbf{w}_{ext} , does the clamp slide down the pipe, or does it remain fixed in place? The figure uses moment labeling to represent the composite wrench cone of contact forces that can act on the clamp from the pipe. The wrench \mathbf{w}_{ext} acting on the clamp can be exactly balanced by a wrench in the composite wrench cone. This is evident from the fact that the wrench opposing \mathbf{w}_{ext} passes around the + labeled region in a counterclockwise sense, meaning that it is contained in the contact wrench cone. As a result, static equilibrium (the \mathbf{ff} contact mode) is a feasible solution for the pipe clamp. To arrive at the same result using an LCSP, label the unit wrenches at the edges of the friction cones $\mathbf{w}_1, \dots, \mathbf{w}_4$. Then the clamp can remain at rest if there exist coefficients a_1, \dots, a_4 such that

$$\begin{aligned} a_1, a_2, a_3, a_4 &\geq 0 \\ a_1 \mathbf{w}_1 + a_2 \mathbf{w}_2 + a_3 \mathbf{w}_3 + a_4 \mathbf{w}_4 + \mathbf{w}_{\text{ext}} &= \mathbf{0}. \end{aligned}$$

To show that static equilibrium is the only solution, all other contact modes must be ruled out. Note that if the friction coefficient at the contacts is too small, the clamp will fall under \mathbf{w}_{ext} .

Analysis of the classic peg-in-hole problem is similar to that of the pipe clamp. Figure 27.7(a) shows an angled peg making two-point contact with the hole. If we apply the wrench \mathbf{w}_1 , the forces from the two-point contact cannot resist, so the \mathbf{ff} contact mode is not a possibility, and the peg will continue to move into the hole.

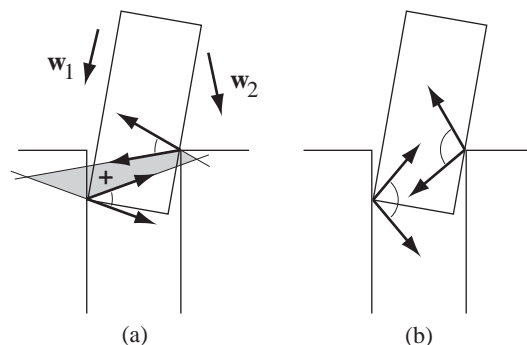


Figure 27.7: (a) The peg will proceed into the hole under the external wrench \mathbf{w}_1 but will get stuck under the wrench \mathbf{w}_2 . (b) The peg is wedged.

If we apply the wrench \mathbf{w}_2 , however, the contacts can resist, and the peg will get stuck. This is called *jamming* [75]. If there is higher friction at the contacts, as in Figure 27.7(b), then each friction cone may be able to “see” the base of the other, and the feasible contact wrenches span the entire wrench space [60]. In this case, any wrench we apply may be resisted by the contacts. The peg is said to be *wedged* [75]. Whether or not the peg will actually resist our applied wrench depends on how much internal force acts between the contacts. This cannot be answered by our rigid-body model; it requires a compliant contact model, as discussed in Section 27.6.

As a slightly more complex quasistatic example, consider a block on a table being pushed by a finger that moves horizontally to the left (Figure 27.8) [49, 88]. Does the part begin to tip over, slide, or both tip and slide? The corresponding contact modes are \mathbf{fbs}_r , $\mathbf{s}_\ell \mathbf{s}_\ell \mathbf{f}$, and $\mathbf{s}_\ell \mathbf{bs}_r$, as shown in Figure 27.8. The figure also shows the composite contact wrench cones using moment labels. It is clear that quasistatic balance between the gravitational force and the wrench cone can only occur for the tipping without slipping contact mode \mathbf{fbs}_r . Therefore, the only quasistatic solution is that the block begins to tip without sliding, and the speed of this motion is determined by the speed of the finger's motion. The graphical construction can be used to confirm our intuition that tipping of the block occurs if we push high on the block or if the friction coefficient at the block's support is high. Try it by pushing a can or glass. Quasistatically, the height of the center of mass is immaterial.

A final example is given in Figure 27.9. A part of mass m and friction coefficient μ is supported by a horizontal surface that moves periodically in the horizontal direc-

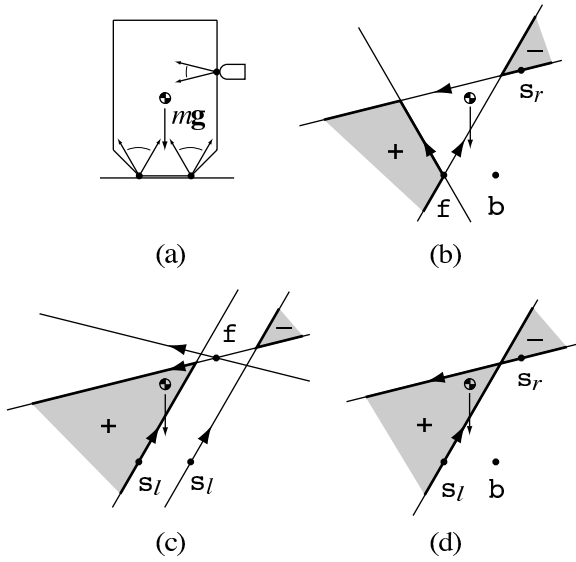


Figure 27.8: (a) A finger moves left into a planar block resting on a table in gravity. The contact friction cones are shown. (b) Possible contact forces for the contact label \mathbf{f} at the leftmost bottom contact, \mathbf{b} at the rightmost bottom contact, and \mathbf{s}_r at the pushing contact. This contact mode $\mathbf{f}\mathbf{b}\mathbf{s}_r$ corresponds to the block tipping over the leftmost contact. Note that the contact wrench cone (represented by moment labels) can provide a force that exactly balances the gravitational force. Thus this contact mode is quasistatically possible. (c) The contact wrench cone for the $\mathbf{s}_\ell\mathbf{s}_\ell\mathbf{f}$ contact mode (block slides left on the table) cannot balance the gravitational force. This contact mode is not quasistatically possible. (d) The contact wrench cone for the $\mathbf{s}_\ell\mathbf{b}\mathbf{s}_r$ contact mode (block slides and tips) is not quasistatically possible.

tion. The periodic motion consists of a large negative acceleration for a short duration and a smaller positive acceleration for a longer duration. The horizontal friction force that can be applied to the part is bounded by $\pm\mu mg$, so the part’s horizontal acceleration is bounded by $\pm\mu g$. As a result, the part cannot keep up with the surface as it accelerates backward. Instead, the part slips forward with respect to the surface, which means the maximal friction force acts in the negative direction, and the part attempts to slow down to the surface’s velocity. Eventually the part catches up with the surface as it executes its slow forward acceleration, which is less than μg . Once the part catches up to the surface, it sticks to it, until the next backward acceleration phase.

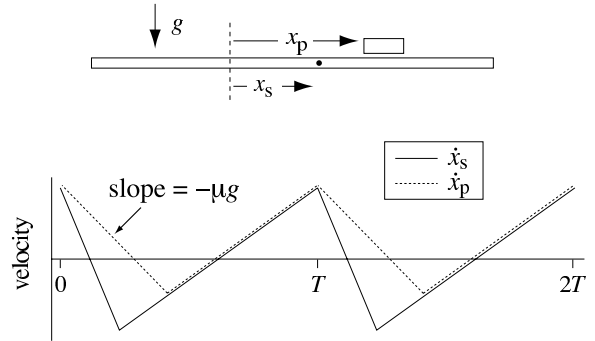


Figure 27.9: (Top) A part supported by horizontally vibrating surface. (Bottom) Friction between the part and the surface causes the part to always try to “catch up” to the surface, but its acceleration is bounded by $\pm\mu g$. The asymmetric motion of the surface gives the part an average positive velocity over a cycle.

As is evident in Figure 27.9, the average part velocity over a cycle is positive, so the part moves forward on the surface [68, 66]. This idea can be extended to create a wide variety of frictional force fields on a rigid plate vibrated with three degrees of freedom in a horizontal plane [69, 70] or with a full six degrees of freedom [83].

For further examples of manipulation planning using the rigid-body model with Coulomb friction, see [55] and the references therein.

27.5 Pushing Manipulation

The friction limit surface (Section 27.7) is useful for analyzing pushing manipulation, as it describes the friction forces that can occur as a part slides over a support surface. When the part is pushed with a wrench contained within the limit surface, friction between the part and the support resists the pushing wrench and the part remains motionless. When the part slides quasistatically, the pushing wrench \mathbf{w} lies on the limit surface, and the part’s twist \mathbf{t} is normal to the limit surface at \mathbf{w} . See Figure 27.10. When the part translates without rotating, the friction force magnitude is μmg , where m is the part’s mass and g is gravitational acceleration. The force applied by the part to the surface is directed through the part’s center of mass in the direction of translation.

If the pushing wrench makes positive moment about the part’s center of mass, the part will rotate counterclockwise (CCW), and if it makes negative moment

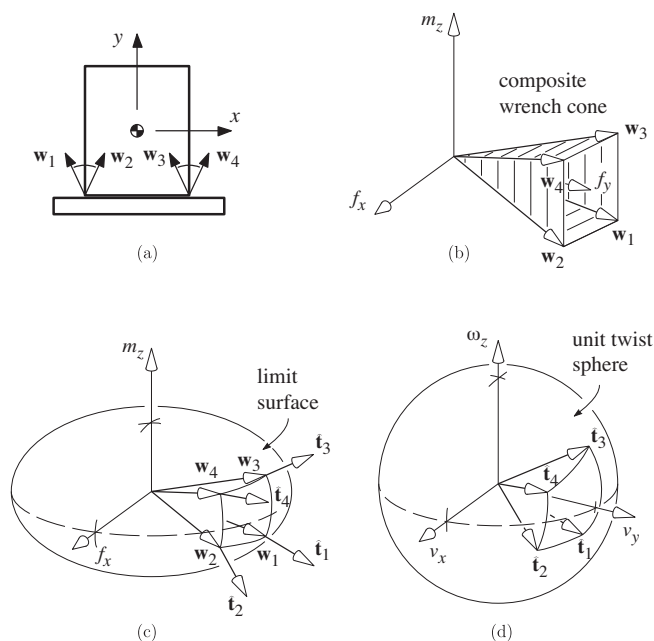


Figure 27.10: (a) Contact between a pusher and a sliding object. (b) The composite contact wrench cone. (c) Mapping the wrench cone through the limit surface to twists of the object. (d) The unit twists that can result from forces in the composite wrench cone.

about the part’s center of mass, it will rotate clockwise (CW). Similarly, if the contact point on the part moves along a line that passes around the part’s center of mass in a CW (respectively CCW) sense, then the part will rotate CW (CCW). From these two observations and considering all possible contact modes, we can conclude that a part pushed at a point contact will rotate CW (CCW) if either (1) both edges of the contact friction cone pass CW (CCW) about the center of mass, or (2) one edge of the friction cone and the pushing direction at the contact both pass around the center of mass in a CW (CCW) sense [53, 55]. See Figure 27.11.

This observation allows pushing to be used to reduce uncertainty in part orientation. A series of pushes with a flat fence can be used to completely eliminate the uncertainty in the orientation of a polygonal part [53, 24, 10]. Bounds on the rate of rotation of parts [2, 55, 64] allows the use of a sequence of stationary fences suspended above a conveyor belt to orient parts by pushing them as they are carried along by the conveyor [65, 9]. *Stable* pushing plans (Figure 27.12) use pushing motions that are guaranteed to keep the part fixed to the pusher as it

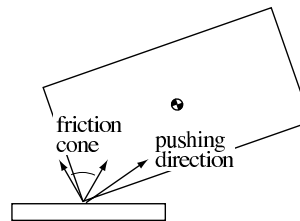


Figure 27.11: The pusher’s motion direction “votes” for counterclockwise rotation of the part, but it is outvoted by the two edges of the friction cone, which both indicate clockwise rotation.

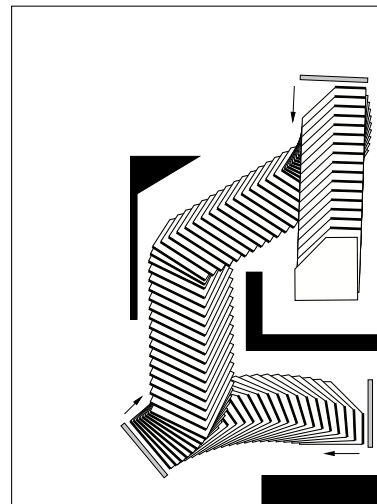


Figure 27.12: Stable pushes can be used to maneuver a part among obstacles.

moves, even in the face of uncertainty in the part’s pressure distribution [48, 51, 55]. Extensions of this work find pushing motions for planar assemblies of parts so that they remain fixed in their relative configurations during motion [31, 6, 7].

The examples above assume that pushing forces and support friction forces act in the same plane. Other work on pushing has considered three-dimensional effects, where pushing forces are applied above the support plane [56].

27.6 Contact Interfaces and Modeling

Contact interface is a general expression to describe the kinematics and kinetics of contacts. Contact applies in various contexts in robotics research; thus, it is more meaningful to refer to generic contact as an “interface,” which is not limited to fingers in grasping and manipulation. The concept of “contact interface” extends the traditional context of physical *contact*. It refers to an interface which imparts the kinematic filtering as well as the duality of force/motion transmitted across the contact interface.

Consequently, contact interface, whether it is rigid or deformable, can be considered as a “kinematic filter” which includes two characteristics: (i) motion and force transmission, and (ii) kinematic duality between force/moment and motion. Different contact interface will be described in the following sections.

Previous sections of this chapter have assumed rigid bodies in contact. In reality, however, all contacts are accompanied by some deformation of the objects. Often this is by design, as in the case of compliant robot fingertips. When deformation is non-negligible, elastic contact models can be used.

27.6.1 Modeling of contact interface

Contact modeling depends on the nature of bodies in contact including material properties, applied force, contact deformation, and elastic properties. This section discusses different contact models.

Rigid-body and point contact models

With the rigid-body assumption, as discussed in the previous sections of this chapter, two models are often used: (i) *point contact without friction* and (ii) *point contact with friction*. In the former case, the contact can only apply force in the direction normal to the contact. In the latter case, a tangential friction force is applied in addition to the normal force. The simplest analytical model for point contact with friction is the Coulomb friction model as presented in equation (27.9).

Hertzian contact model

Elastic contact modeling was first studied and formulated more than a century ago by Hertz in 1882 [32] based on contact between two linear elastic materials

with a normal force which results in very small contact deformation. This is commonly called the *Hertzian* contact and can be found in most mechanics textbooks, such as [39, 81]. Hertz made two important explicit assumptions in order for his contact model to be applicable:

1. objects of linear elastic materials in contact, and
2. small contact deformation compared to the dimension of object.

Hertz also conducted experiments using a spherical glass lens against a planar glass plate to validate the contact theory.

Two relevant results of the Hertzian contact theory applied to robotic contact interfaces are summarized as follows. The first pertains to the radius of the contact area. Hertz [32] studied the growth of the contact area as a function of the applied normal force N based on the linear elastic model. Based on 10 experimental trials, he concluded that the radius of contact is proportional to the normal force raised to the power of $\frac{1}{3}$, which is consistent with the analytical results he derived based on the linear elastic model. That is, the radius of contact, a , is related to the normal force, N , by the equation

$$a \propto N^{\frac{1}{3}}. \quad (27.11)$$

The second result pertains to the pressure distribution over the assumed symmetric contact area—a second-order pressure distribution of the nature of an ellipse or circle. For a symmetric and circular contact area, the pressure distribution is

$$p(r) = \frac{N}{\pi a^2} \sqrt{1 - \left(\frac{r}{a}\right)^2}, \quad (27.12)$$

where N is the normal force, a is the radius of contact, and r is the distance from the center of contact with $0 \leq r \leq a$.

Soft contact model

A typical contact interface between a soft finger and contact surface is illustrated in Figure 27.13. In typical robotic contact interfaces, the materials of the fingertips are not linear elastic. A model that extends linear to non-linear elastic contact was presented in [87] with a power-law equation which subsumes the Hertzian contact theory,

$$a = c N^\gamma, \quad (27.13)$$

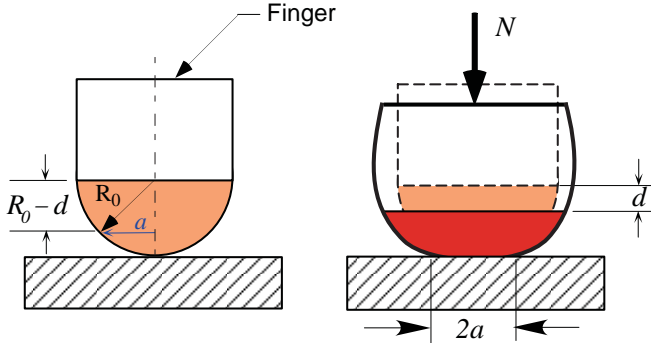


Figure 27.13: An elastic soft fingertip with hemispherical tip making contact with a rigid surface.

where $\gamma = \frac{n}{2n+1}$ is the exponent of the normal force, n is the strain-hardening exponent, and c is a constant depending on the size and curvature of the finger tip as well as the material properties. Equation (27.13) is the new power law that relates the growth of the circular contact radius to the applied normal force for soft fingers. Note that the equation is derived assuming circular contact area. For linear elastic materials, the constant n is equal to 1 with $\gamma = \frac{1}{3}$, resulting in the Hertzian contact model in equation (27.11). Therefore, the soft contact model in equation (27.13) subsumes the Hertzian contact model.

Other models

Other models include anthropomorphic contacts and visco-elastic contacts. In modeling visco-elastic contacts, the creep or relaxation phenomenon is incorporated with a time dependent function, in addition to the elastic deformation described in the general equation (27.13).

27.6.2 Kinematic duality in contact modeling

At each contact, the force and velocity constraints can be represented by an $n \times 6$ *constraint* or *selection* matrix, \mathbf{H} [16], at the contact interface. This constraint matrix works like a filter to transmit or deny certain components of motion across the contact interface. In the same token, forces/moments applied across the contact interface are also filtered by the same constraint matrix, \mathbf{H}^T , in a dual relationship. Three typical contact models are illustrated in the following.

- The *point contact without friction* model. Only a

normal force, f_z , can be exerted between the contacting bodies:

$$f_z \geq 0 \quad \mathbf{f} = \mathbf{H}^T f_z = [0 \ 0 \ 1 \ 0 \ 0 \ 0]^T f_z \quad (27.14)$$

- The *point contact with friction* model includes tangential friction forces, f_x and f_y , in addition to normal force, f_z ,

$$f_z \geq 0; |f_t| = \sqrt{f_x^2 + f_y^2} \leq \mu f_z;$$

$$\mathbf{f} = \mathbf{H}^T \begin{bmatrix} f_x \\ f_y \\ f_z \end{bmatrix} = \begin{bmatrix} 1 & 0 & 0 \\ 0 & 1 & 0 \\ 0 & 0 & 1 \\ 0 & 0 & 0 \\ 0 & 0 & 0 \\ 0 & 0 & 0 \end{bmatrix} \begin{bmatrix} f_x \\ f_y \\ f_z \end{bmatrix} \quad (27.15)$$

where f_x and f_y are the x - and y -components of the tangential contact force, and f_z is the normal force.

- The *soft finger* contact model with a finite contact patch, allows in addition to the friction and normal forces a torsional moment with respect to the contact normal [34, 41, 35, 87, 42]. The kinematic equations are

$$f_z \geq 0;$$

$$\mathbf{f} = \mathbf{H}^T \begin{bmatrix} f_x \\ f_y \\ f_z \\ m_z \end{bmatrix} = \begin{bmatrix} 1 & 0 & 0 & 0 \\ 0 & 1 & 0 & 0 \\ 0 & 0 & 1 & 0 \\ 0 & 0 & 0 & 0 \\ 0 & 0 & 0 & 0 \\ 0 & 0 & 0 & 1 \end{bmatrix} \begin{bmatrix} f_x \\ f_y \\ f_z \\ m_z \end{bmatrix} \quad (27.16)$$

where m_z is the moment with respect to the normal of contact. The finite contact area assumed by the soft contact interface results in the application of a friction moment in addition to the traction forces. If the resultant force on the tangential plane of contact is denoted as $f_t = \sqrt{f_x^2 + f_y^2}$ and the moment with respect to the contact normal is m_z , the following elliptical equation represents the relationship between the force and moment at the onset of sliding:

$$\frac{f_t^2}{a^2} + \frac{m_z^2}{b^2} = 1 \quad (27.17)$$

where $a = \mu N$ is the maximum friction force, and $b = (m_z)_{max}$ is the maximum moment. Further readings on this subject can be found in [37, 28, 34, 41, 35, 87, 42, 80].

Table 27.1: Duality of the kinematics of contact interface: the force/motion relationships for finger and grasped object are dual to each other in the joint space, contact interface, and the Cartesian space of the object.

motion	$\mathbf{J}_\theta \quad \delta\theta = \delta\mathbf{x}_f$ (6xm)(mx1) (6x1)	$\mathbf{H} \quad \delta\mathbf{x}_f = \delta\mathbf{x}_{tr} = \mathbf{H} \quad \delta\mathbf{x}_p$ (nx6)(6x1) (nx1) (nx6)(6x1)	$\mathbf{J}_c \quad \delta\mathbf{x}_b = \delta\mathbf{x}_p$ (6x6)(6x1) (6x1)
	\longleftrightarrow	\longleftrightarrow	
	JOINTS	CONTACT	OBJECT
force	$\mathbf{J}_\theta^T \quad \mathbf{f}_f = \tau$ (mx6) (6x1) (mx1)	$\mathbf{f}_f = \mathbf{H}^T \quad \mathbf{f}_{tr} = \mathbf{f}_p$ (6x1) (6xn) (nx1) (6x1)	$\mathbf{J}_c^T \quad \mathbf{f}_p = \mathbf{f}_b$ (6x6) (6x1) (6x1)

As can be appreciated from the three cases above, the rows of \mathbf{H} are the directions along which contact forces are supported. Conversely, relative motions of the two objects are constrained along these same directions: $\mathbf{H}\dot{q} = 0$. Thus, the constraint matrix works like a kinematic filter which dictates the components of motions that can be transmitted through the contact interface. The introduction of this matrix makes it easy to model the contact mechanics in analysis using the dual kinematic relationship between force/moment and motion, as described in Table 27.1. For example, the constraint filter matrix in equation (27.16) describes that all three components of forces and one component of the moment with respect to the normal of contact can be transmitted through the contact interface of a soft finger.

In Chapter 28, when multiple contact is considered, such \mathbf{H} matrices associated with each finger can be concatenated in an augmented matrix to work in conjunction with the grasp and Jacobian matrices for the analysis of grasping and manipulation.

Table 27.1 summarizes the dual relationship between the force/moment and displacement—a result that is derived from the principle of virtual work. In Table 27.1, \mathbf{J}_θ is the joint Jacobian matrix relating joint velocities to fingertip velocities, and \mathbf{J}_c is the Cartesian coordinate transformation matrix relating the contact point with the centroidal coordinates of the grasped object. In addition, the number of degree of freedom (dof) in the task space is n and the number of dof in the joint spaces is m .

27.6.3 Pressure distribution at contacts

In Section 27.6.1, when the Hertzian contact theory is considered, the assumed pressure distribution for small elastic deformation is given in equation (27.12). As the radius of curvature of the two asperities increases and the material properties change to hyper-elastic, the pressure

k	coefficient C_k
$k = 2$ (circular)	$C_2 = 1.5$
$k = 3$ (cubic)	$C_3 = 1.24$
$k = 4$ (quadruple)	$C_4 = 1.1441$
$k \rightarrow \infty$ (uniform)	$C_\infty = 1.0$

 Table 27.2: Table of the coefficient of the pressure distribution equation (27.18), C_k

distribution becomes more uniform [85, 61, 87]. Generalizing equation (27.12), the pressure distribution function for circular contact area with radius a is

$$p(r) = C_k \frac{N}{\pi a^2} \left[1 - \left(\frac{r}{a}\right)^k \right]^{\frac{1}{k}}, \quad (27.18)$$

where N is the normal force, a is the radius of contact, r is the radius with $0 \leq r \leq a$, k determines the shape of the pressure profile, and C_k is a coefficient which adjusts for the profile of pressure distribution over the contact area to satisfy the equilibrium condition. In equation (27.18), $p(r)$ is defined for $0 \leq r \leq a$. By symmetry, $p(r) = p(-r)$ when $-a \leq r \leq 0$, as shown in Figure 27.14. When k becomes larger, the pressure distribution approaches uniform distribution, as shown in Figure 27.14. It is also required that the integral of the pressure over the contact area be equal to the normal force; that is,

$$\int_R p(r) dA = \int_{\theta=0}^{2\pi} \int_{r=0}^a p(r) r dr d\theta = N. \quad (27.19)$$

The coefficient C_k can be obtained by substituting equation (27.18) into equation (27.19). It is interesting to note that when equation (27.19) is integrated, both the normal force and radius of contact vanish, leaving only the constant C_k as follows

$$C_k = \frac{3}{2} \frac{k \Gamma(\frac{3}{k})}{\Gamma(\frac{1}{k}) \Gamma(\frac{2}{k})}, \quad (27.20)$$

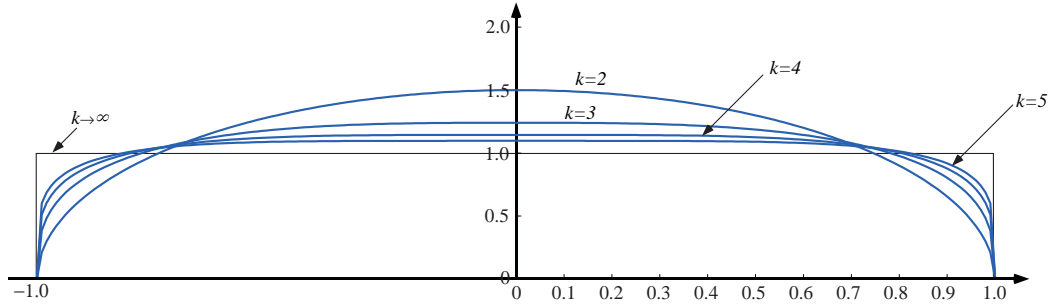


Figure 27.14: Illustration of pressure distribution with respect to the normalized radius, r/a . The plot shows axisymmetric pressure distribution with $k = 2, 3, 4, 5$ and ∞ . As k increases, the pressure profile will become more uniform.

where $k = 1, 2, 3, \dots$ are typically integer values (although non-integer k values are also possible) and $\Gamma()$ is the Gamma function [1]. The numerical values of C_k for a few values of k are listed in Table 27.2 for reference. A normalized pressure distribution with respect to the normalized radius, r/a , is plotted in Figure 27.14. As can be seen from the figure, when k approaches infinity, the pressure profile will become that of a uniformly distributed load with magnitude of $\frac{N}{\pi a^2}$, in which case $C_k = 1.0$.

For linear elastic materials, $k = 2$ can be used although it is found that $k \cong 1.8$ is also appropriate in some cases [40]. For nonlinear elastic and visco-elastic materials, the value of k tends to be higher, depending on the properties of the material.

27.7 Friction Limit Surface

Friction “limit surface” is a conceptual surface within which sliding does not occur; that is, the limit surface is the boundary between non-sliding vs. sliding motions in grasping and manipulation. The normal to the limit surface also is the instantaneous direction of sliding. Depending on contact types, friction limit surface takes different shapes.

For example, a planar contact patch occurs when a flat object slides on the floor, a soft robot finger presses against a face of a polyhedron, or a foot of a humanoid robot pushes on the ground. It is of interests for us to know what forces can be transmitted through such a contact and if certain magnitudes of forces and moment will cause sliding at the contact interface.

For ease of discussion, we will call one of the objects in contact the “part” (e.g., the flat object on the floor

or the robot finger) and the other object a stationary “support.” We define a coordinate frame so that the planar contact patch is in the $z = 0$ plane, and let $p(\mathbf{r}) \geq 0$ be the contact pressure distribution between the part and support as a function of the location $\mathbf{r} = (x, y)$. The friction coefficient at the contact patch is μ . If the planar velocity of the part is $\mathbf{t} = [\omega_z, v_x, v_y]^T$, then the linear velocity at \mathbf{r} is

$$\mathbf{v}(\mathbf{r}) = (v_x - \omega_z y, v_y + \omega_z x),$$

and the unit velocity is $\hat{\mathbf{v}}(\mathbf{r}) = \mathbf{v}(\mathbf{r})/\|\mathbf{v}(\mathbf{r})\|$. The infinitesimal force applied by the part to the support at \mathbf{r} , in the plane of sliding, is

$$d\mathbf{f}(\mathbf{r}) = (df_x(\mathbf{r}), df_y(\mathbf{r})) = \mu p(\mathbf{r}) dA \hat{\mathbf{v}}(\mathbf{r}). \quad (27.21)$$

The total wrench the part applies to the support is

$$\mathbf{w} = \begin{bmatrix} m_z \\ f_x \\ f_y \end{bmatrix} = \int_A \begin{bmatrix} x df_y(\mathbf{r}) - y df_x(\mathbf{r}) \\ df_x(\mathbf{r}) \\ df_y(\mathbf{r}) \end{bmatrix} dA, \quad (27.22)$$

where A is the support area.

As expected, the wrench is independent of the speed of motion: for a given \mathbf{t}_0 and all $\alpha > 0$, the wrench resulting from velocities $\alpha \mathbf{t}_0$ is identical. Viewing equation (27.22) as a mapping from twists to wrenches, we can map the surface of the unit twist sphere ($\|\hat{\mathbf{t}}\| = 1$) to a surface in the wrench space. This surface is called the *limit surface* [27, 29], and it is closed, convex, and encloses the origin of the wrench space (Figure 27.10(c)). The portion of the wrench space enclosed by this surface is exactly the set of wrenches the part can transmit to the support. When the part slips on the support ($\mathbf{t} \neq \mathbf{0}$), the contact wrench \mathbf{w} lies on the limit surface, and by the maximum work inequality, the twist \mathbf{t} is normal to the limit

surface at \mathbf{w} . If the pressure distribution $p(\mathbf{r})$ is finite everywhere, the limit surface is smooth and strictly convex, and the mapping from unit twists to unit wrenches, and vice-versa, is continuous and one-to-one. The limit surface also satisfies the property $\mathbf{w}(-\hat{\mathbf{t}}) = -\mathbf{w}(\hat{\mathbf{t}})$.

Section 27.7.1 discusses limit surface of point contacts. Section 27.7.2 presents a way to numerically construct friction limit surface of soft contacts using the kinematic concept of COR. Section 27.7.3 illustrates the construction of friction limit surface with an example.

27.7.1 Friction limit surface for point contact with friction

The 3D limit surface for point contact with friction, governed by the Coulomb's law, is illustrated by the 3D friction cone in Figure 27.4, with the boundary of the friction limit surface described by the following equation

$$f_t = \mu N \quad \text{or} \quad \sqrt{f_x^2 + f_y^2} = \mu f_z \quad (27.23)$$

where f_t is the friction force, $\mu = \tan \beta$ is the coefficient of friction, and N is the normal force. If the tangential plane is aligned with the xy plane, the second part of equation (27.23) will apply.

27.7.2 The friction limit surface at a soft contact interface

Given a pressure distribution² in equation (27.18), we can numerically construct the corresponding friction limit surface by using equations (27.21) and (27.22).

In the following, we will exploit the kinematic property of center of rotation (COR) with modeling symmetry to formulate equations for the magnitudes of friction force and moment on a circular contact patch. Figure 27.15 shows a circular contact patch with an instantaneous center of rotation (COR). By moving (or scanning) the COR along the X -axis, different possible combinations of friction force and moment can be obtained to construct the limit surface. More details can be found in [38, 34, 26, 27, 29, 41, 35, 87, 80].

The following derivation is for the total friction force (f_t) and moment (m_z) on the contact interface for the COR at a distance d_c along the X -axis, as shown in Figure 27.15. By varying the COR distance d_c from $-\infty$ to ∞ , all possible combinations of (f_t, m_z) can be found in order to construct the entire friction limit surface.

²When Hertzian contact pressure distribution [32] is considered, use $k = 2$ in equation (27.18).

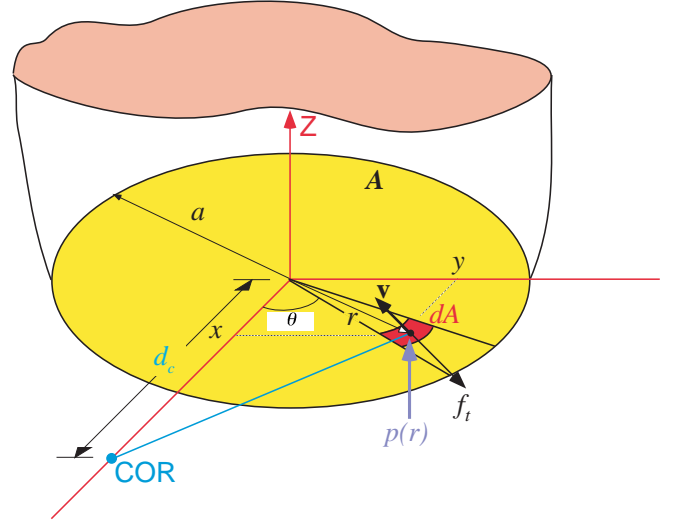


Figure 27.15: Contact and coordinates for COR and local infinitesimal area dA for numerical integration to construct the limit surface of soft fingers.

The tangential force over the entire contact area can be obtained by integrating shear force on each infinitesimal areas, dA , on which the Coulomb's law of friction is observed³, over the entire contact area, A . Setting $\mathbf{r} = [x \ y]^T$ and $r = \|\mathbf{r}\|$, the total tangential force can be integrated using equation (27.21) to obtain:

$$\mathbf{f}_t = \begin{bmatrix} f_x \\ f_y \end{bmatrix} = - \int_A \mu \hat{\mathbf{v}}(\mathbf{r}) p(r) dA \quad (27.24)$$

where A denotes the circular contact region in Figure 27.15, \mathbf{f}_t is the tangential force vector with the direction shown in Figure 27.15, μ is the coefficient of friction, $\hat{\mathbf{v}}(\mathbf{r})$ is the unit vector in the direction of the velocity vector $\mathbf{v}(\mathbf{r})$ with respect to the COR on the infinitesimal area dA at the location \mathbf{r} , $p(r)$ is the pressure distribution at distance r from the center of contact⁴. The minus sign denotes the opposite directions of $\hat{\mathbf{v}}(\mathbf{r})$ and \mathbf{f}_t . Since we are primarily interested in the magnitude of the friction force and moment, we shall omit the sign in the later derivation when magnitudes are concerned.

Similarly, the moment about the z -axis, or the normal to the contact area, is

$$m_z = \int_A \mu \|\mathbf{r} \times \hat{\mathbf{v}}(\mathbf{r})\| p(r) dA, \quad (27.25)$$

³For infinitesimal contact area, the contact resembles a point contact. Hence, the Coulomb's law of friction can be employed.

⁴Since the pressure along the annular ring with distance r from the center is the same, we denote it as $p(r)$ instead of $p(\mathbf{r})$.

where $\|\mathbf{r} \times \hat{\mathbf{v}}(\mathbf{r})\|$ is the magnitude of the cross product of the vectors \mathbf{r} and $\hat{\mathbf{v}}(\mathbf{r})$, whose direction is normal to the contact surface.

The unit vector $\hat{\mathbf{v}}(\mathbf{r})$ is related to the distance d_c from the origin to the COR chosen on the X -axis from Figure 27.15, and can be written as follows

$$\begin{aligned}\hat{\mathbf{v}}(\mathbf{r}) &= \frac{1}{\sqrt{(x-d_c)^2 + y^2}} \begin{bmatrix} -y \\ (x-d_c) \end{bmatrix} \\ &= \frac{1}{\sqrt{(r \cos \theta - d_c)^2 + (r \sin \theta)^2}} \begin{bmatrix} -r \sin \theta \\ (r \cos \theta - d_c) \end{bmatrix}.\end{aligned}\quad (27.26)$$

Due to symmetry, $f_x = 0$ for all COR's along the X -axis; therefore, the magnitude of the tangential force in the contact tangent plane is $f_t = f_y$. Substituting equations (27.18) and (27.26) into (27.24) and (27.25), we obtain

$$f_t = \int_A \mu \frac{(r \cos \theta - d_c)}{\sqrt{r^2 + d_c^2 - 2r d_c \cos \theta}} C_k \frac{N}{\pi a^2} \left[1 - \left(\frac{r}{a}\right)^k\right]^{\frac{1}{k}} dA. \quad (27.27)$$

Similarly, the moment about the axis normal to the plane is

$$m_z = \int_A \mu \frac{r^2 - r d_c \cos \theta}{\sqrt{r^2 + d_c^2 - 2r d_c \cos \theta}} C_k \frac{N}{\pi a^2} \left[1 - \left(\frac{r}{a}\right)^k\right]^{\frac{1}{k}} dA. \quad (27.28)$$

In equations (27.27) and (27.28), polar coordinates are defined such that $x = r \cos \theta$, $y = r \sin \theta$, and $dA = r dr d\theta$. We also introduce a normalized coordinate

$$\tilde{r} = \frac{r}{a}. \quad (27.29)$$

From equation (27.29), we can write $dr = a d\tilde{r}$. We also denote $\tilde{d}_c = \frac{d_c}{a}$, and assume that μ is constant throughout the contact area. Substituting the normalized coordinate into equation (27.27) and dividing both sides by μN , we can derive

$$\frac{f_t}{\mu N} = \frac{C_k}{\pi} \int_0^{2\pi} \int_0^1 \frac{(\tilde{r}^2 \cos \theta - \tilde{r} \tilde{d}_c)}{\sqrt{\tilde{r}^2 + \tilde{d}_c^2 - 2\tilde{r} \tilde{d}_c \cos \theta}} (1 - \tilde{r}^k)^{\frac{1}{k}} d\tilde{r} d\theta. \quad (27.30)$$

Substituting again $\tilde{r} = \frac{r}{a}$ and $dr = a d\tilde{r}$ into equation (27.28) and normalizing with $a\mu N$, we obtain

$$\frac{m_z}{a\mu N} = \frac{C_k}{\pi} \int_0^{2\pi} \int_0^1 \frac{(\tilde{r}^3 \cos \theta - \tilde{r}^2 \tilde{d}_c)}{\sqrt{\tilde{r}^2 + \tilde{d}_c^2 - 2\tilde{r} \tilde{d}_c \cos \theta}} (1 - \tilde{r}^k)^{\frac{1}{k}} d\tilde{r} d\theta. \quad (27.31)$$

Equations (27.30) and (27.31) can be numerically integrated for a distance d_c or \tilde{d}_c to yield a point on the limit surface for a prescribed pressure distribution $p(r)$ given by equation (27.18). Both equations involve elliptic integrals whose closed form solutions may not exist

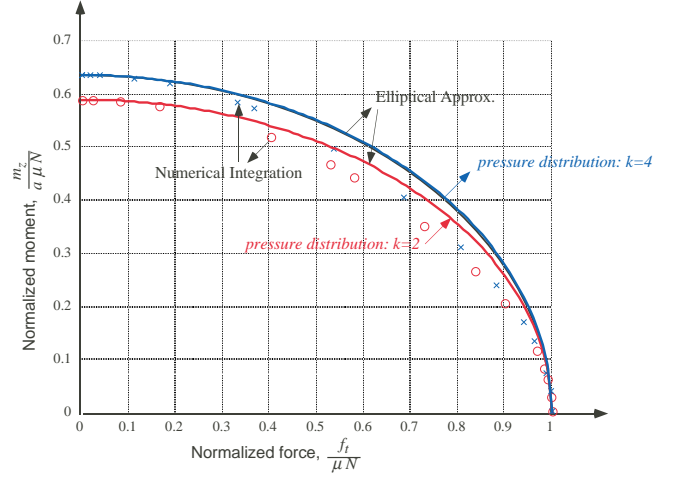


Figure 27.16: Example: Limit surface obtained by numerical integration and elliptical approximation. The numerical integration is based on the pressure distribution, $p(r)$, and the coefficient, C_k . In this figure, the pressure distributions in equation (27.18) of both $k = 2$ and $k = 4$ are used.

but can be evaluated numerically. When the COR distance d_c varies from $-\infty$ to ∞ , all possible combinations of (f_t, m_z) can be obtained for plotting the friction limit surface.

27.7.3 Example of constructing a friction limit surface

When the pressure distribution is fourth-order with $k = 4$, the coefficient from Table 27.2 is $C_4 = \frac{6}{\sqrt{\pi}} \frac{\Gamma(3/4)}{\Gamma(1/4)} = 1.1441$. Equations (27.30) and (27.31) can be written as

$$\frac{f_t}{\mu N} = 0.3642 \int_0^{2\pi} \int_0^1 \frac{(\tilde{r}^2 \cos \theta - \tilde{r} \tilde{d}_c)}{\sqrt{\tilde{r}^2 + \tilde{d}_c^2 - 2\tilde{r} \tilde{d}_c \cos \theta}} (1 - \tilde{r}^4)^{\frac{1}{4}} d\tilde{r} d\theta.$$

$$\frac{m_z}{a\mu N} = 0.3642 \int_0^{2\pi} \int_0^1 \frac{(\tilde{r}^3 \cos \theta - \tilde{r}^2 \tilde{d}_c)}{\sqrt{\tilde{r}^2 + \tilde{d}_c^2 - 2\tilde{r} \tilde{d}_c \cos \theta}} (1 - \tilde{r}^4)^{\frac{1}{4}} d\tilde{r} d\theta.$$

Numerical integration for different values of \tilde{d}_c yields pairs of $(\frac{f_t}{\mu N}, \frac{m_z}{a\mu N})$. Plots of these pairs are shown in Figure 27.16.

A reasonable approximation to these numerical results is given by the following equation of ellipse

$$\left[\frac{f_t}{\mu N}\right]^2 + \left[\frac{m_z}{(m_z)_{max}}\right]^2 = 1, \quad (27.32)$$

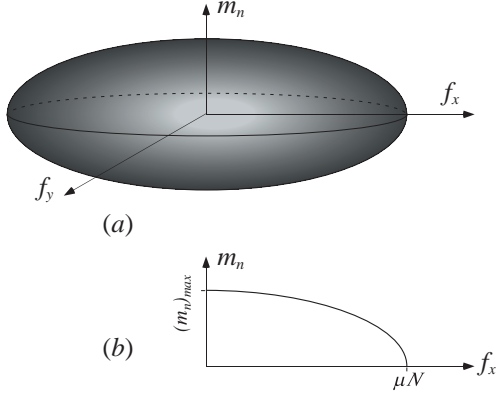


Figure 27.17: Friction limit surface for soft fingers: (a) a 3D ellipsoid representing the limit surface, and (b) a section of the ellipsoidal limit surface showing the coupled relationship between the force and moment.

where the maximum moment $(m_z)_{max}$ is

$$(m_z)_{max} = \int_A \mu r C_k \frac{N}{\pi a^2} \left[1 - \left(\frac{r}{a} \right)^k \right]^{\frac{1}{k}} dA.$$

obtained by equation (27.28) with the COR at $d_c = 0$. This defines the quarter-elliptical curves in Figure 27.16. This approximation is the basis for constructing a 3D ellipsoidal limit surface, as illustrated in Figure 27.17, and is a good model for the soft contact described in Section 27.6.1. More details can be found in [37, 29, 34, 41, 35, 42, 80].

27.8 Contacts in Grasping and Fixture Designs

It is often important to relate the force and contact displacement (or deformation of contact interface) in grasping and fixture design in which deformable contacts are concerned. Furthermore, such force-displacement relationship is typically nonlinear due to the nature of contact. A linear expression such as the Hooke's law cannot capture the instantaneous and overall characteristics of force and displacement for these contacts. In this section, we formulate and discuss such relationship using the elastic contact model.

From Figure 27.13 and the geometry of contact, equation (27.13), relating the contact radius with normal force, can be rewritten. Assuming $d \ll R_0$, the following equation can be derived [42]

$$N = c_d d^\zeta \quad (27.33)$$

where c_d is a proportional constant, and ζ is

$$\zeta = \frac{1}{2\gamma}. \quad (27.34)$$

Both c_d and ζ can be obtained experimentally. The exponent ζ can also be obtained from γ through equation (27.34) if γ is already known for the fingertip. The range of the exponent in equation (27.33) is $\frac{3}{2} \leq \zeta < \infty$. In equation (27.33), the approach or the vertical depression of the fingertip, d , is proportional to the normal force raised to the power of 2γ (cf. equation (27.34)) which ranges from 0 to $\frac{2}{3}$.

A plot of normal force versus displacement of contact is shown in Figure 27.18 using equation (27.33) with nonlinear power-law equation. Experimental data of contact between a soft finger and flat surface show consistent results when compared with Figure 27.18 [42].

27.8.1 Contact stiffness of soft fingers

The nonlinear contact stiffness of a soft finger is defined as the ratio of the change in normal force with respect to the change in vertical depression at the contact. The contact stiffness of soft fingers can be obtained by differentiating equation (27.33) as follows

$$k_s = \frac{\partial N}{\partial d} = c_d \zeta d^{\zeta-1} = \zeta \left(\frac{N}{d} \right). \quad (27.35)$$

Substitute equation (27.33) with $d = \left(\frac{N}{c_d} \right)^{1/\zeta}$ into equation (27.35) to derive

$$k_s = c_d^{\frac{1}{\zeta}} \zeta N^{\frac{\zeta-1}{\zeta}} = c_d^{2\gamma} \zeta N^{1-2\gamma}. \quad (27.36)$$

Thus, the nonlinear contact stiffness of soft fingers, derived in a succinct form in equation (27.35), is the product of the exponent ζ and the ratio of the normal force versus the approach, N/d . A typical contact stiffness as a function of vertical depression is plotted in Figure 27.18. The stiffness shown in the figure increases with the force. The expressions for the stiffness, k_s , as a function of various parameter(s) are summarized in the following table.

	$f(d)$	$f(N)$	$f(N, d)$
k_s	$c_d \zeta d^{\zeta-1}$	$c_d^{\frac{1}{\zeta}} \zeta N^{\frac{\zeta-1}{\zeta}}$	$\zeta \left(\frac{N}{d} \right)$

The change in stiffness can be obtained by differentiating equation (27.35) to derive the following equations:

$$\frac{\partial k_s}{\partial d} = c_d \zeta (\zeta - 1) d^{\zeta-2} \quad (27.37)$$

$$\frac{\partial k_s}{\partial N} = \frac{\zeta - 1}{d}. \quad (27.38)$$

Description	Equation for soft fingers	Parameters
power law	$a = cN^\gamma$	$0 \leq \gamma \leq \frac{1}{3}$
pressure distribution	$p(r) = p(0) \left[1 - \left(\frac{r}{a}\right)^k\right]^{\frac{1}{k}}$	typically $k \geq 1.8$
contact approach	$N = c_d d^\zeta$	$\frac{3}{2} \leq \zeta \leq \infty$
contact stiffness	$k_s = \zeta \frac{N}{d}$	nonlinear

Table 27.3: Summary of the contact mechanics equations for linear elastic (when $\gamma = \frac{1}{3}$ or $\zeta = \frac{3}{2}$) and nonlinear elastic soft fingers.

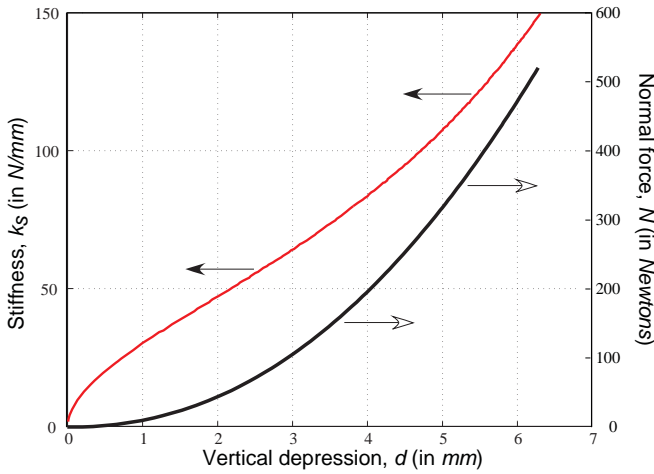


Figure 27.18: The typical load-depression curve in equation (27.33) shown with a scale to the right, and the contact stiffness, k_s , as given by equation (27.35) with a scale to the left.

Equation (27.35) suggests that the stiffness of soft contacts always increases because the ratio N/d always increases, with constant ζ for prescribed fingertip material and range of normal force. This is consistent with the observation that the contact stiffness becomes larger (i.e., stiffer) with larger depression and force. Additionally, equation (27.38) suggests that the contact stiffness, k_s , always increases with the normal force because $\frac{\partial k_s}{\partial N} > 0$ owing to $\zeta \geq 1.5$. Moreover, the change in stiffness with respect to the normal load is inversely proportional to the vertical depression, d , as derived in equation (27.38). This result asserts that the rate of increase in the contact stiffness will gradually become less and less as the normal load and vertical depression increase.

A summary of the equations for soft fingers is presented in Table 27.3. The range of the exponent of the general power-law equation in (27.13) is $0 \leq \gamma \leq \frac{1}{3}$. The Hertzian contact has an exponent of $\gamma = \frac{1}{3}$; therefore,

the Hertzian contact theory for linear elastic materials is a special case of equation (27.13). Linear elastic materials, such as steel or other metallic fingertips, under small deformation generally follow the Hertzian contact theory fairly well. The power-law equation in (27.13) should be employed for fingertips made of softer materials, such as soft rubber or silicone or even visco-elastic fingertips.

27.8.2 Application of soft contact theory to fixture design

The preceding analysis and results can be applied in fixturing design and other applications that involve contact with finite areas (for example, [45]). In fixture design with soft contact (e.g., copper surfaces) under relatively large deformation and load, the power-law equations in Table 27.3 should be considered in place of the Hertzian contact equation. In these cases, the Hertzian contact model is no longer accurate and should be replaced. On the other hand, if linear elastic materials are used in fixture design with relatively small deformation ($\frac{d}{R_0} \leq 5\%$), the exponent should be taken as $\gamma = \frac{1}{3}$ when applying the contact theory. Furthermore, the exponent γ was found to be material-dependent and not geometry-dependent in general [87]. Once the value of γ is determined for the material (for example, using a tensile testing machine with the experimental procedure in [87]), it can be employed for the analysis of fixturing design using the relevant equations presented herewith.

27.9 Further Reading

Mason’s textbook [55] expands on a number of themes in this chapter, including the theory of polyhedral convex cones, graphical methods for planar problems, and applications to manipulation planning. Fundamental material on polyhedral cones can be found in [25] and their application to representations of twists and wrenches

in [21, 22, 23, 33]. Twists and wrenches are elements of classical *screw theory*, which is covered in the texts [4, 36] and from the point of view of robotics in the texts [58, 19, 74].

In addition, several relevant chapters in this handbook provide further reading for theory and applications, for example, chapters 1 and 28.

Bibliography

- [1] M. Abramowitz and I. Stegun. *Handbook of Mathematical Functions with formulas, graphs, and mathematical tables*. Dover, 7th edition, 1972.
- [2] J. C. Alexander and J. H. Maddocks. Bounds on the friction-dominated motion of a pushed object. *International Journal of Robotics Research*, 12(3):231–248, 1993.
- [3] M. Anitescu and F. Potra. Formulating multi-rigid-body contact problems with friction as solvable linear complementarity problems. *ASME Journal of Nonlinear Dynamics*, 14:231–247, 1997.
- [4] R. S. Ball. *The Theory of Screws*. Cambridge University Press, 1900.
- [5] S. Berard, J. Trinkle, B. Nguyen, B. Roghani, J. Fink, and V. Kumar. daVinci code: A multi-model simulation and analysis tool for multi-body systems. In *IEEE International Conference on Robotics and Automation*, 2007.
- [6] J. D. Bernheisel and K. M. Lynch. Stable transport of assemblies: Pushing stacked parts. *IEEE Transactions on Automation Science and Engineering*, 1(2):163–168, 2004.
- [7] J. D. Bernheisel and K. M. Lynch. Stable transport of assemblies by pushing. *IEEE Transactions on Robotics*, 22(4):740–750, August 2006.
- [8] A. Bicchi. On the problem of decomposing grasp and manipulation forces in multiple whole-limb manipulation. *Int. Jour. of Robotics and Autonomous Systems*, vol. 13, 1994.
- [9] M. Brokowski, M. Peshkin, and K. Goldberg. Curved fences for part alignment. In *IEEE International Conference on Robotics and Automation*, pages 3:467–473, Atlanta, GA, 1993.
- [10] R. C. Brost. Automatic grasp planning in the presence of uncertainty. *International Journal of Robotics Research*, 7(1):3–17, February 1988.
- [11] C. Cai and B. Roth. On the spatial motion of a rigid body with point contact. In *IEEE International Conference on Robotics and Automation*, pages 686–695, 1987.
- [12] C. S. Cai and B. Roth. On the planar motion of rigid bodies with point contact. *Mechanism and Machine Theory*, 21(6):453–466, 1986.
- [13] A. B. A. Cole, J. E. Hauser, and S. S. Sastry. Kinematics and control of multifingered hands with rolling contact. *IEEE Transactions on Automatic Control*, 34(4):398–404, April 1989.
- [14] R. W. Cottle, J.-S. Pang, and R. E. Stone. *The Linear Complementarity Problem*. Academic Press, 1992.
- [15] C. A. Coulomb. Théorie des machines simples en ayant égard au frottement de leurs parties et à la roideur des cordages. *Mémoires des mathématique et de physique présentés à l’Académie des Sciences*, 1781.
- [16] M. R. Cutkosky and I. Kao. Computing and controlling the compliance of a robotic hand. *IEEE Transaction on Robotics and Automation*, 5(2):151–165, April 1989.
- [17] M. R. Cutkosky and S. H. Lee. Fixture planning with friction for concurrent product/process design. In *NSF process planning*, 1989.
- [18] K. Dandekar and A. K. Srinivasan. A 3-dimensional finite element model of the monkey fingertip for predicting responses of slowly adapting mechanoreceptors. In *ASME Bioengineering Conference*, volume 29, pages 257–258, 1995.
- [19] J. K. Davidson and K. H. Hunt. *Robots and Screw Theory*. Oxford University Press, 2004.
- [20] P. E. Dupont. The effect of Coulomb friction on the existence and uniqueness of the forward dynamics problem. In *IEEE International Conference on*

- Robotics and Automation*, pages 1442–1447, Nice, France, 1992.
- [21] M. A. Erdmann. A configuration space friction cone. In *IEEE/RSJ International Conference on Intelligent Robots and Systems*, pages 455–460, Osaka, Japan, 1991.
- [22] M. A. Erdmann. Multiple-point contact with friction: Computing forces and motions in configuration space. In *IEEE/RSJ International Conference on Intelligent Robots and Systems*, pages 163–170, Yokohama, Japan, 1993.
- [23] M. A. Erdmann. On a representation of friction in configuration space. *International Journal of Robotics Research*, 13(3):240–271, 1994.
- [24] K. Y. Goldberg. Orienting polygonal parts without sensors. *Algorithmica*, 10:201–225, 1993.
- [25] A. J. Goldman and A. W. Tucker. Polyhedral convex cones. In H. W. Kuhn and A. W. Tucker, editors, *Linear Inequalities and Related Systems*. Princeton University Press, 1956.
- [26] S. Goyal, A. Ruina, and J. Papadopoulos. Limit surface and moment function description of planar sliding. In *Proceedings of 1989 IEEE International Conference on Robotics and Automation*, pages 794–799, Scottsdale, Arizona, May 1989.
- [27] S. Goyal, A. Ruina, and J. Papadopoulos. Planar sliding with dry friction. Part 1. Limit surface and moment function. *Wear*, 143:307–330, 1991.
- [28] S. Goyal, A. Ruina, and J. Papadopoulos. Planar sliding with dry friction: Part 2. dynamics of motion. *Wear*, 143:331–352, 1991.
- [29] S. Goyal, A. Ruina, and J. Papadopoulos. Planar sliding with dry friction. Part 2. Dynamics of motion. *Wear*, 143:331–352, 1991.
- [30] K. Harada, M. Kaneko, and T. Tsuji. Rolling based manipulation for multiple objects. In *Proceedings of IEEE Int'l Conf. on Robotics and Automation*, pages 3888–3895, San Francisco, CA, April 2000.
- [31] K. Harada, J. Nishiyama, Y. Murakami, and M. Kaneko. Pushing multiple objects using equivalent friction center. In *IEEE International Conference on Robotics and Automation*, pages 2485–2491, 2002.
- [32] H. Hertz. *On the Contact of Rigid Elastic Solids and on Hardness*, chapter 6: Assorted Papers by H. Hertz. MacMillan, New York, November 1882.
- [33] S. Hirai and H. Asada. Kinematics and statics of manipulation using the theory of polyhedral convex cones. *International Journal of Robotics Research*, 12(5):434–447, 1993.
- [34] R. Howe, I. Kao, and M. Cutkosky. Sliding of robot fingers under combined torsion and shear loading. In *Proceedings of 1988 IEEE International Conference on Robotics and Automation*, volume 1, pages 103–105, Philadelphia, Pennsylvania, April 24–29 1988.
- [35] R. D. Howe and M. R. Cutkosky. Practical force-motion models for sliding manipulation. *International Journal of Robotics Research*, 15(6):555–572, 1996.
- [36] K. H. Hunt. *Kinematic Geometry of Mechanisms*. Oxford University Press, 1978.
- [37] J. Jameson and L. Leifer. Quasi-static analysis: A method for predicting grasp stability. In *Proceedings of 1986 IEEE International Conference on Robotics and Automation*, pages 876–883, April 1986.
- [38] J. W. Jameson. *Analytic Techniques for Automated Grasp*. PhD thesis, Department of Mechanical Engineering, Stanford University, June 1985.
- [39] K. L. Johnson. *Contact Mechanics*. Cambridge University Press, Cambridge, 1985.
- [40] I. Kao, S.-F. Chen, Y. Li, and G. Wang. Application of bio-engineering contact interface and MEMS in robotic and human augmented systems. *IEEE Robotics and Automation Magazine*, 10(1):47–53, March 2003.
- [41] I. Kao and M. R. Cutkosky. Dextrous manipulation with compliance and sliding. *International Journal of Robotics Research*, 11(1):20–40, February 1992.
- [42] I. Kao and F. Yang. Stiffness and contact mechanics for soft fingers in grasping and manipulation. *the IEEE Trans. of Robotics and Automation*, 20(1):132–135, February 2004.
- [43] K. Komvopoulos and D.-H. Choi. Elastic finite element analysis of multi-asperity contacts. *Journal of Tribology*, 114:823–831, 1992.

- [44] S.-H. Lee and M. Cutkosky. Fixture planning with friction. *ASME Journal of Engineering for Industry*, 113(3):320–327, August 1991.
- [45] Q. Lin, J. W. Burdick, and E. Rimon. A stiffness-based quality measure for compliant grasps and fixtures. *IEEE Transactions on Robotics and Automation*, 16(6):675–688, December 2000.
- [46] P. Lötstedt. Coulomb friction in two-dimensional rigid body systems. *Zeitschrift für Angewandte Mathematik und Mechanik*, 61:605–615, 1981.
- [47] P. Lötstedt. Mechanical systems of rigid bodies subject to unilateral constraints. *SIAM Journal of Applied Mathematics*, 42(2):281–296, 1982.
- [48] K. M. Lynch. The mechanics of fine manipulation by pushing. In *IEEE International Conference on Robotics and Automation*, pages 2269–2276, Nice, France, 1992.
- [49] K. M. Lynch. Toppling manipulation. In *IEEE International Conference on Robotics and Automation*, 1999.
- [50] K. M. Lynch and M. T. Mason. Pulling by pushing, slip with infinite friction, and perfectly rough surfaces. *International Journal of Robotics Research*, 14(2):174–183, April 1995.
- [51] K. M. Lynch and M. T. Mason. Stable pushing: Mechanics, controllability, and planning. *International Journal of Robotics Research*, 15(6):533–556, December 1996.
- [52] Y. Madea and T. Arai. Planning of graspless manipulation by a multifingered robot hand. *Advanced Robotics*, 19(5):501–521, June 2005.
- [53] M. T. Mason. Mechanics and planning of manipulator pushing operations. *International Journal of Robotics Research*, 5(3):53–71, Fall 1986.
- [54] M. T. Mason. Two graphical methods for planar contact problems. In *IEEE/RSJ International Conference on Intelligent Robots and Systems*, pages 443–448, Osaka, Japan, November 1991.
- [55] M. T. Mason. *Mechanics of Robotic Manipulation*. MIT Press, 2001.
- [56] H. Mayeda and Y. Wakatsuki. Strategies for pushing a 3D block along a wall. In *IEEE/RSJ International Conference on Intelligent Robots and Systems*, pages 461–466, Osaka, Japan, 1991.
- [57] D. J. Montana. The kinematics of contact and grasp. *The International Journal of Robotics Research*, 7(3):17–32, June 1988.
- [58] R. M. Murray, Z. Li, and S. S. Sastry. *A Mathematical Introduction to Robotic Manipulation*. CRC Press, 1994.
- [59] Y. Nakamura. Contact stability measure and optimal finger force control of multi-fingered robot hands. In *Crossing Bridges: Advances in Flexible Automation and Robotics*, pages 523–528. ASME, The Proceedings of the USA-Japan Symposium on Flexible Automation, July 1988.
- [60] V.-D. Nguyen. Constructing force-closure grasps. *The International Journal of Robotics Research*, 7(3):3–16, June 1988.
- [61] E. J. Nicolson and R. S. Fearing. The reliability of curvature estimates from linear elastic tactile sensors. In *the Proceedings of the 1995 IEEE International Conference on Robotics and Automation*. IEEE Press, 1995.
- [62] J. S. Pang and J. C. Trinkle. Complementarity formulations and existence of solutions of dynamic multi-rigid-body contact problems with Coulomb friction. *Mathematical Programming*, 73:199–226, 1996.
- [63] Y. C. Park and G. P. Starr. Optimal grasping using a multifingered robot hand. In *Proceedings of the 1990 IEEE International Conference on Robotics and Automation*, pages 689–694, Cincinnati, Ohio, May 13–18 1990. IEEE.
- [64] M. A. Peshkin and A. C. Sanderson. The motion of a pushed, sliding workpiece. *IEEE Journal of Robotics and Automation*, 4(6):569–598, December 1988.
- [65] M. A. Peshkin and A. C. Sanderson. Planning robotic manipulation strategies for workpieces that slide. *IEEE Journal of Robotics and Automation*, 4(5):524–531, October 1988.
- [66] A. E. Quaid. A miniature mobile parts feeder: Operating principles and simulation results. In *IEEE International Conference on Robotics and Automation*, pages 2221–2226, 1999.
- [67] F. Reuleaux. *The Kinematics of Machinery*. MacMillan, 1876. Reprinted by Dover, 1963.

- [68] D. Reznik and J. Canny. The Coulomb pump: a novel parts feeding method using a horizontally-vibrating surface. In *IEEE International Conference on Robotics and Automation*, pages 869–874, 1998.
- [69] D. Reznik and J. Canny. A flat rigid plate is a universal planar manipulator. In *IEEE International Conference on Robotics and Automation*, pages 1471–1477, 1998.
- [70] D. Reznik and J. Canny. C'mon part, do the local motion! In *IEEE International Conference on Robotics and Automation*, pages 2235–2242, 2001.
- [71] E. Rimon and J. Burdick. On force and form closure for multiple finger grasps. In *IEEE International Conference on Robotics and Automation*, pages 1795–1800, 1996.
- [72] E. Rimon and J. W. Burdick. New bounds on the number of frictionless fingers required to immobilize planar objects. *Journal of Robotic Systems*, 12(6):433–451, 1995.
- [73] E. Rimon and J. W. Burdick. Mobility of bodies in contact—part I: A 2nd-order mobility index for multiple-finger grasps. *IEEE Transactions on Robotics and Automation*, 14(5):696–708, October 1998.
- [74] J. M. Selig. *Geometric Fundamentals of Robotics, 2nd edition*. Springer, 2005.
- [75] S. N. Simunovic. Force information in assembly processes. In *International Symposium on Industrial Robots*, 1975.
- [76] P. Song, J.-S. Pang, and V. Kumar. A semi-implicit time-stepping model for frictional compliant contact problems. *International Journal for Numerical Methods in Engineering*, 60(13):2231–2261, 2004.
- [77] T. H. Speeter. Three-dimensional finite element analysis of elastic continua for tactile sensing. *International Journal of Robotics Research*, 11(1):1–19, Feb 1992.
- [78] D. Stewart and J. Trinkle. An implicit time-stepping scheme for rigid body dynamics with inelastic collisions and Coulomb friction. *International Journal for Numerical Methods in Engineering*, 39:2673–2691, 1996.
- [79] L. T. Tenek and J. Argyris. *Finite Element Analysis for Composite Structures*. Kluwer Academic Publishers, 1998.
- [80] P. Tiezzi and I. Kao. Modeling of viscoelastic contacts and evolution of limit surface for robotic contact interface. *IEEE Transaction on Robotics*, 23(2):206–217, April 2007.
- [81] S. P. Timoshenko and J. N. Goodier. *Theory of Elasticity*. McGraw-Hill Book Company, 3rd edition, 1970.
- [82] J. C. Trinkle, J. S. Pang, S. Sudarsky, and G. Lo. On dynamic multi-rigid-body contact problems with Coulomb friction. *Zeitschrift für Angewandte Mathematik und Mechanik*, 77(4):267–279, 1997.
- [83] T. Vose, P. Umbanhowar, and K. M. Lynch. Vibration-induced frictional force fields on a rigid plate. In *IEEE International Conference on Robotics and Automation*, 2007.
- [84] Y.-T. Wang, V. Kumar, and J. Abel. Dynamics of rigid bodies undergoing multiple frictional contacts. In *Proceedings of IEEE Int'l Conf. on Robotics and Automation*, pages 2764–2769, 1992.
- [85] E. Wolf. *Progress in Optics*, volume XXX. North-Holland, 1992.
- [86] N. Xydias, M. Bhagavat, and I. Kao. Study of soft-finger contact mechanics using finite element analysis and experiments. In *Proc. IEEE Int. Conf. on Robotics and Automation, ICRA*, San Francisco, California, 2000.
- [87] N. Xydias and I. Kao. Modeling of contact mechanics and friction limit surface for soft fingers with experimental results. *International Journal of Robotic Research*, 18(9):941–950, September 1999.
- [88] M. T. Zhang, K. Goldberg, G. Smith, R.-P. Berretty, and M. Overmars. Pin design for part feeding. *Robotica*, 19(6):695–702, 2001.